HHS Public Access

Author manuscript

Cell Rep. Author manuscript; available in PMC 2023 January 17.

Published in final edited form as:

Cell Rep. 2021 November 23; 37(8): 110054. doi:10.1016/j.celrep.2021.110054.

Protein kinase Cι and SRC signaling define reciprocally related subgroups of glioblastoma with distinct therapeutic vulnerabilities

Rajappa S. Kenchappa[1,8,*], **Yi Liu**[1,8], **Michael G. Argenziano**[2], **Matei A. Banu**[2], **Ann C. Mladek**[3], **Rita West**[1], **Amanda Luu**[1], **Alfredo Quiñones-Hinojosa**[4], **Dolores Hambardzumyan**[5], **Verline Justilien**[1], **Michael Leitges**[6], **Jann N. Sarkaria**[3], **Peter A. Sims**[7], **Peter Canoll**[2], **Nicole R. Murray**[1,*], **Alan P. Fields**[1,*], **Steven S. Rosenfeld**[1,9,*]

[1]Department of Cancer Biology, Mayo Clinic, Jacksonville, FL 32224, USA

[2]Department of Pathology and Cell Biology, Columbia University Medical Center, New York, NY 10032, USA

[3]Department of Radiation Oncology, Mayo Clinic, Rochester, MN 55902, USA

[4]Department of Neurosurgery, Mayo Clinic, Jacksonville, FL 32224, USA

[5]Departments of Neurosurgery and Oncological Sciences, Mount Sinai School of Medicine, New York, NY 10029, USA

[6]Memorial University of Newfoundland, St. John's, NL, Canada

[7]Department of Systems Biology, Columbia University Medical Center, New York, NY 10032, USA

[8]These authors contributed equally

[9]Lead contact

SUMMARY

We report that atypical protein kinase Cι (PKCι) is an oncogenic driver of glioblastoma (GBM). Deletion or inhibition of PKCι significantly impairs tumor growth and prolongs survival in murine GBM models. GBM cells expressing elevated PKCι signaling are sensitive to PKCι inhibitors, whereas those expressing low PKCι signaling exhibit active SRC signaling and sensitivity to SRC inhibitors. Resistance to the PKCι inhibitor auranofin is associated with activated SRC signaling and response to a SRC inhibitor, whereas resistance to a SRC inhibitor is associated with activated

[*]Correspondence: kenchappa.rajappa@mayo.edu (R.S.K.), murray.nicole@mayo.edu (N.R.M.), fields.alan@mayo.edu (A.P.F.), rosenfeld.steven@mayo.edu (S.S.R.).

AUTHOR CONTRIBUTIONS

Conception and design: R.S.K., S.S.R., P.C., P.A.S., A.P.F., and N.R.M.; development of methodology: R.S.K., S.S.R., V.J., A.P.F., N.R.M., P.C., and P.A.S.; acquisition of data: R.S.K., Y.L., R.W., A.L., M.G.A., M.A.B., and V.J.; analysis and interpretation of data: R.S.K., Y.L., S.S.R., A.P.F., N.R.M., P.C., P.A.S., M.G.A., and M.A.B.; administrative, technical, or material support: A.C.M., A.Q.-H., D.H., M.L., and J.N.S.

DECLARATION OF INTERESTS

The authors declare no competing interests.

SUPPLEMENTAL INFORMATION

Supplemental information can be found online at https://doi.org/10.1016/j.celrep.2021.110054.

PKCι signaling and sensitivity to auranofin. Interestingly, PKCι- and SRC-dependent cells often co-exist in individual GBM tumors, and treatment of GBM-bearing mice with combined auranofin and SRC inhibitor prolongs survival beyond either drug alone. Thus, we identify PKCι and SRC signaling as distinct therapeutic vulnerabilities that are directly translatable into an improved treatment for GBM.

In brief

Kenchappa et al. demonstrate that the tumor cells that comprise a glioblastoma, the most common and lethal of brain tumors, can be distinguished by how they depend on two oncogenic kinases: PKCι and SRC.

Graphical Abstract

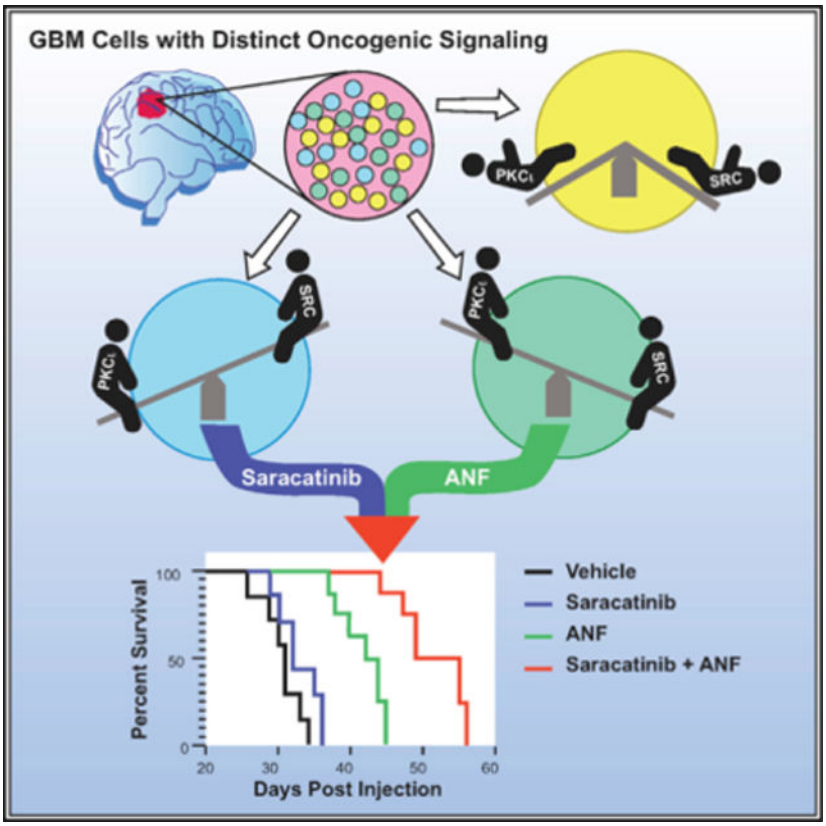

INTRODUCTION

Glioblastoma (GBM) is among the most common and lethal of primary brain tumors (Puduvalli and Hoang, 2018). Effective treatment options are limited, and 5-year survival averages 3%–7%. This poor outlook is due in part to the redundancy in oncogenic signaling pathways that are pathogenic in GBM (Dong et al., 2020; Olmez et al., 2018). Signal redundancy may explain why highly specific and potent tyrosine kinase inhibitors have failed to demonstrate clinical efficacy, even with drugs that penetrate the blood-brain barrier (BBB) (De Witt Hamer, 2010; Reardon et al., 2015; Szerlip et al., 2012). Protein kinase

Cι (PKCι; gene name *PRKCI*) is an oncogenic kinase that is overexpressed and activated in many malignancies, including GBM (Liu et al., 2020a; Parker et al., 2014). Although genetic silencing of *PRKCI* in GBM cells reduces invasion and proliferation *in vitro* (Baldwin et al., 2008; Desai et al., 2011, 2012), the role of PKCι in GBM is unknown. We have shown that PKCι is required for growth and invasion of lung, pancreatic, and ovarian cancer cells (Regala et al., 2005a, 2005b; Scotti et al., 2010, 2012; Wang et al., 2013). PKCι activates multiple oncogenic signaling pathways, including MEK-ERK (Frederick et al., 2008), Hedgehog (Justilien et al., 2014), Notch (Ali et al., 2016), and ribosome biogenesis (Justilien et al., 2017a, 2017b). In addition, we have identified auranofin, a US Food and Drug Administration (FDA)-approved drug, as a potent and selective inhibitor of PKCι signaling (Erdogan et al., 2006; Stallings-Mann et al., 2006). Auranofin is currently in clinical trials for treatment of leukemia and several solid malignancies (Jatoi et al., 2015; Mansfield et al., 2013). In this study, we use genetically engineered mouse models (GEMMs), human GBM cell lines, and patient-derived xenografts (PDXs) to investigate the role of PKCι in GBM. Our results have broad therapeutic implications for improving the efficacy of targeted therapeutics in this disease.

RESULTS

Characterization of PKCι-dependent oncogenic signaling in GBM

PKCι is activated in many tumor types by tumor-specific copy number alterations of its encoding gene, *PRKCI* (Liu et al., 2020a). To determine whether PKCι plays a role in GBM biology, we assessed *PRKCI* copy number, *PRKCI* RNA expression, and PKCι pathway activity in human GBM. We divided The Cancer Genome Atlas (TCGA) GBM dataset into two groups: one corresponding to the 25% of GBMs with the highest *PRKCI* mRNA levels (*Top25*) and the other corresponding to the 25% with the lowest (*Btm25*). The *Top25* group expressed significantly higher *PRKCI* than the *Btm25* group (Figure 1A) and was significantly enriched in tumors with *PRKCI* copy number gains (CNGs) ($p = 0.0008$) (Figure 1B, black bars). Conversely, the *Btm25* group was enriched in tumors with monoallelic loss of *PRKCI* ($p < 0.05$) (Figure 1B, white bars). Chromosome 3q26 CNG drives amplification of *PRKCI* and its two downstream 3q26 targets, *ECT2* and *SOX2*, resulting in coordinate overexpression of *PRKCI* and *ECT2* RNA in virtually all human tumor types analyzed (Liu et al., 2020a). In contrast, 3q26 CNG drives overexpression of *SOX2* mRNA in only some tumor types, particularly squamous cell tumors (Liu et al., 2020a). Analysis of the TCGA GBM dataset reveals that *PRKCI*, *ECT2*, and *SOX2* are subject to coordinate CNG and monoallelic loss in GBM tumors (Figures S1A and S1B). CNG results in overexpression of *PRKCI* and *ECT2*, but not *SOX2* mRNA, whereas monoallelic loss leads to a trend toward reduced *PRKCI* and *ECT2* RNA expression, but no change in *SOX2* (Figures S1C–S1E). We previously characterized two key oncogenic PKCι signaling pathways: the PKCι-ECT2-ribosome biogenesis pathway (Justilien et al., 2017a) and the PKCι-MEK-ERK signaling pathway (Frederick et al., 2008; Regala et al., 2005a) (Figure 1C). We next assessed whether the *Top25* and *Btm25* groups of human GBMs differ in expression of gene signatures associated with these pathways. A PKCι-dependent ECT2 pathway signature consisting of 12 ribosomal processing genes whose expression is highly correlated with PKCι expression and PKCι-dependent ribosomal DNA transcription (Table

S1; Justilien et al., 2017a, 2017b) was used to interrogate PKCι-ECT2 pathway activity. To interrogate the PKCι-MEK-ERK pathway, we defined a PKCι-dependent MEK pathway signature in GBM consisting of the 13 leading edge genes that drive the enrichment of the Kyoto Encyclopedia of Genes and Genomes (KEGG) mitogen-activated protein kinase (MAPK) pathway in the *Top25* group of GBM tumors (Table S1; Figure S1F). We then calculated a PKCι-dependent ECT2 pathway score and a PKCι-dependent MEK pathway score for all tumors in the TCGA GBM dataset. The *Top25* group exhibited significantly higher ECT2 and MEK pathway scores than the *Btm25* group (Figures S1G and S1H), and both pathway scores exhibit significant positive correlations with *PRKCI* expression in the entire TCGA GBM dataset (Figures 1D and 1E). These data indicate that elevated *PRKCI* expression in human GBMs drives activation of both the PKCι-ECT2 and the PKCι-MEK signaling pathways, consistent with our findings in other malignancies (Liu et al., 2020a; Yin et al., 2019).

Tumor PKCι protein expression predicts PKCι signaling activity in human GBM

To assess whether tumor PKCι protein abundance correlates with PKCι-ECT2 and PKCι-MEK pathway activity in primary GBM tumors, we performed PKCι immunohistochemistry (IHC) on tissue microarrays (TMAs) containing 68 human GBMs and 9 normal control brain samples and calculated PKCι immunoscores for these tissues. PKCι expression was assessed by IHC and found to be significantly elevated in the majority of GBMs compared with normal brain (Figure 1F). Specificity of staining was confirmed by the fact that staining was lost when primary PKCι antibody was omitted (Figures S2A and S2B). Interrogation of the subset of GBM samples for which RNA sequencing (RNA-seq) data were also available (n = 42) reveals a significant positive correlation between PKCι immunoscore and both *PRKCI* mRNA abundance (Figure 1G) and Ki67 immunoscore (Figure 1H). Finally, ECT2 and MEK pathway scores correlate positively with PKCι immunoscore across this GBM dataset (Figures 1I and 1J).

PKCι protein expression predicts sensitivity to PKCι inhibitors

We next assessed the effects of two PKCι inhibitors, auranofin and CRT0066854, on the viability of a panel of human and murine GBM cell lines (Figures 2A and 2B; Table S2). Auranofin is an FDA-approved drug that blocks PKCι-dependent transformed growth (Ali et al., 2016; Justilien et al., 2017a; Liu et al., 2020b) by disrupting its interaction with PAR6 (Erdogan et al., 2006; Regala et al., 2008; Stallings-Mann et al., 2006). CRT0066854 is a highly selective ATP-competitive PKCι inhibitor (Kjær et al., 2013). Interestingly, responses to both inhibitors reveal a significant inverse relationship between PKCι protein abundance and EC_{50} (Figures 2C and 2D). These results are consistent with our previous finding that *PRKCI* expression correlates positively with sensitivity to auranofin in other solid tumors (Liu et al., 2020b; Regala et al., 2008). Moreover, we observed a strong, positive correlation between auranofin and CRT006854 sensitivities among these cell lines (Figure S2C), indicating that the growth-inhibitory activity of both drugs is mediated through PKCι inhibition. We next evaluated whether auranofin sensitivity and PKCι expression are correlated in cell lines derived from four representative human GBM PDX models that express either high or low PKCι (Figure 2E). The two high PKCι-expressing cell lines are more sensitive to auranofin than the low PKCι-expressing cell lines (Figure 2F, compare red

versus green; Table S2), consistent with our findings in human and mouse GBM cell lines (Figures 2C and 2D). Thus, PKCι expression correlates with response to PKCι inhibitors in both mouse and human GBM cells.

PRKCI CNG and PKCι signaling are associated with progression of low-grade gliomas to GBM

GBMs have traditionally been classified into classical, mesenchymal, and proneural subgroups (Verhaak et al., 2010). Analysis of the TCGA dataset reveals that proneural tumors exhibit significantly higher *ECT2* pathway scores than the other two subtypes (Figure S3A). However, because this classification scheme has not been useful in guiding clinical decision making, we analyzed *PRKCI* copy number and signaling using data from a study that identified genomic features predicting progression of low-grade glioma (LGG) to GBM (Ceccarelli et al., 2016). This study divided LGGs into *IDH* wild-type and mutant groups. The *IDH* wild-type group was further divided into four subtypes: classical-like, mesenchymal-like, LGm6-GBM, and PA-like, with the first three showing much poorer survival than the last (Ceccarelli et al., 2016). Although *PRKCI* CNGs were present at similar frequencies in the first three subtypes, they were absent from the PA-like subtype (Figure S3B). Consistent with PKCι pathway activation, the three subtypes exhibiting poor survival and *PRKCI* CNG show significantly higher *ECT2* pathway score than PA-like tumors (Figure S3C). We observed a similar association when we analyzed the IDH mutant group, which is subdivided into three subtypes: Codel, G-CIMP-high, and G-CIMP-low. The Codel and G-CIMP-high subtypes show little potential to progress to GBM, while the G-CIMP-low subtype has a significantly higher propensity to do so. Interestingly, only the aggressive G-CIMP-low subtype harbors significant *PRKCI* CNGs (Figure S3D) and significantly elevated ECT2 pathway score (Figure S3E), when compared with the less aggressive Codel and G-CIMP-high subtypes. Finally, survival analysis of the entire cohort reveals that *PRKCI* CNG is significantly associated with reduced survival (Figure S3F). Taken together, these data provide compelling evidence that *PRKCI* CNG and activated PKCι signaling are strongly associated with progression of LGG to GBM.

Genetic loss of *Prkci* inhibits tumor growth and invasion and extends survival in two murine GBM models

The data above indicate that PKCι may play a critical role in the transformed phenotype of GBM. To examine the role of PKCι in GBM tumorigenesis, we crossed mice harboring conditional knockout (cKO) alleles for *Pten* or *Trp53* with those harboring cKO alleles of *Prkci* to generate $Trp53^{fl/fl}$, $Trp53^{fl/fl}/Prkci^{fl/fl}$, $Pten^{fl/fl}$, and $Pten^{fl/fl}/Prkci^{fl/fl}$ mice. Injection of a bicistronic retrovirus encoding hemagglutinin (HA)-tagged *PDGF* and *Cre* recombinase into the white matter of these mice leads to recombination of the cKO alleles with subsequent development of GBMs exhibiting a proneural phenotype (Figure 3A, left panel) (Lei et al., 2011). Mice harboring $Trp53^{-/-}/Prkci^{-/-}$ and $Pten^{-/-}/Prkci^{-/-}$ tumors exhibited significantly increased median survival when compared with their $Trp53^{-/-}$ and $Pten^{-/-}$ tumor-bearing counterparts (Figure 3A, right panel). At endpoint, both $Trp53^{-/-}$ and $Trp53^{-/-}/Prkci^{-/-}$ GBMs contain areas of necrosis, a prominent histologic feature of human GBM (Figure 3B, upper panels). IHC reveals robust PKCι expression in $Trp53^{-/-}$ GBMs and its absence in $Trp53^{-/-}/Prkci^{-/-}$ GBMs, whereas the surrounding brain in both

genotypes stains positively for PKCι, confirming tumor-specific knockout of *Prkci* in *Trp53*$^{-/-}$/*Prkci*$^{-/-}$ GBMs (Figure 3B, lower panels). At 14 days after retroviral injection, *Trp53*$^{-/-}$/*Prkci*$^{-/-}$ GBMs are significantly smaller and less dispersed than *Trp53*$^{-/-}$ tumors ($p = 0.023$, two-tailed t test; Figure S5A; Figure 3C), indicating that *Prkci* promotes both tumor growth and invasion.

To assess whether the decrease in growth and invasion in *Trp53*$^{-/-}$/*Prkci*$^{-/-}$ tumors reflects intrinsic properties of these GBM cells, we derived stable cell lines from three *Trp53*$^{-/-}$ and three *Trp53*$^{-/-}$/*Prkci*$^{-/-}$ GBM tumors and confirmed the absence of PKCι expression in *Trp53*$^{-/-}$/*Prkci*$^{-/-}$ GBM cells (Figure 3D). *In vitro* invasion was measured for three independently derived *Trp53*$^{-/-}$ and *Trp53*$^{-/-}$/*Prkci*$^{-/-}$ cell lines (Figure 3E, blue versus red). Although one-way ANOVA found highly significant differences between cell lines ($p < 0.0001$), post hoc pairwise comparisons confirmed only significant ($p < 0.05$) differences in Transwell invasion between the three *Trp53*$^{-/-}$/*Prkci*$^{-/-}$ cell lines and one *Trp53*$^{-/-}$ line (line 3). Likewise, although one-way ANOVA for doubling times (Figure 3F) was highly significant ($p = 0.003$), post hoc pairwise comparisons confirmed significantly longer doubling times for *Trp53*$^{-/-}$/*Prkci*$^{-/-}$ lines 1 and 3 ($p < 0.05$) compared with the three *Trp53*$^{-/-}$ lines. This variability in migration and proliferation behavior *in vitro* may reflect differential activation of other signaling pathways that can regulate growth and invasion in response to deletion of PKCι. Finally, we find that *Trp53*$^{-/-}$ GBM cells exhibit elevated levels of phosphorylated ECT2 (Figure 3G), phospho-ERK (Figure 3H), and active RAC1 (Figure 3I) (Justilien and Fields, 2009; Justilien et al., 2011) when compared with *Trp53*$^{-/-}$/*Prkci*$^{-/-}$ GBM cells, consistent with the role of PKCι in activating these oncogenic pathways.

PKCι inhibitors suppress growth and invasion of mouse *Trp53*$^{-/-}$ GBM cells *in vitro*

Our data above indicate that PKCι plays a key promotive role in the growth and invasion of mouse GBM tumor cells *in vivo* and *in vitro*. Therefore, we next assessed the effect of PKCι inhibition on *Trp53*$^{-/-}$ GBM cells. Three independently derived *Trp53*$^{-/-}$ cell lines exhibit dose-dependent auranofin-mediated inhibition of cell viability with EC_{50} values between 49 and 62 nM (Figure 4A), while EC_{50}s for *Trp53*$^{-/-}$/*Prkci*$^{-/-}$ cell lines are 5- to 40-fold higher (Table S2). At higher concentrations, auranofin can inhibit thioredoxin reductase (TR), leading to cytotoxicity through oxidative stress (Roder and Thomson, 2015). To assess whether TR inhibition contributes to the growth-inhibitory effects of auranofin, we treated *Trp53*$^{-/-}$ and *Trp53*$^{-/-}$/*Prkci*$^{-/-}$ cells with auranofin ± *N*-acetyl cysteine (NAC), a reactive oxygen scavenger. Although NAC has little impact on *Trp53*$^{-/-}$ cell viability at auranofin concentrations <200 nM (Figure 4B), it does inhibit toxicity of higher doses of auranofin in *Trp53*$^{-/-}$/*Prkci*$^{-/-}$ cells (Figure 4C). Furthermore, the ATP-competitive PKCι inhibitor CRT0066854 (Kjær et al., 2013) reduces cell viability of *Trp53*$^{-/-}$ cells with an EC_{50} ~95 nM but has essentially no effect on the viability of *Trp53*$^{-/-}$/*Prkci*$^{-/-}$ cells (Figure 4D). Thus, the effects of auranofin on *Trp53*$^{-/-}$ GBM cells at doses <200 nM reflect PKCι inhibition. Consistent with this conclusion, auranofin treatment leads to a rapid and sustained decrease in ERK and ECT2 phosphorylation (Figure 4E). Similar results were obtained with CRT0066854 (Figure S2D). Furthermore, acute treatment with auranofin

markedly and uniformly reduces invasion of each of the three *Trp53*$^{-/-}$ cell lines (Figure 4F, closed versus open symbols).

SRC signaling is activated in GBMs expressing low *PRKCI*

Because *Trp53*$^{-/-}$/*Prkci*$^{-/-}$ mice eventually succumb to GBM (Figure 3A), both PKCι-dependent and -independent pathways can support GBM tumorigenesis. To identify pathway(s) activated in the presence of low *PRKCI*, we performed gene set enrichment analysis (GSEA) on the *Top25* and *Btm25* human GBM groups (Table S3). SRC signaling emerged as the most significantly enriched oncogenic signature in the *Btm25* group (Table S3; Figure S4A). To validate this association, we generated a *SRC* pathway signature consisting of the leading edge SRC pathway genes identified by GSEA (Table S1) and calculated *SRC* pathway scores for all tumors in the dataset. Results confirmed that the *Btm25* group exhibited significantly higher *SRC* pathway scores than the *Top25* group (Figure S4B). Furthermore, the *SRC* pathway score showed a significant negative correlation with *PRKCI* expression, *ECT2* pathway score, and *MEK* pathway score across the entire TCGA GBM dataset (Figures 5A–5C). Heatmap analysis revealed that the *Top25* and *Btm25* human GBM groups can be defined by a reciprocal relationship between the activities of PKCι and SRC oncogenic signaling (Figure 5D). Consistent with this relationship, murine *Trp53*$^{-/-}$/*Prkci*$^{-/-}$ GBM cells exhibit significantly elevated levels of activated, Y418 phosphorylated SRC when compared with *Trp53*$^{-/-}$ GBM cells (Figure 5E), indicating that the SRC pathway is activated in the absence of *Prkci*. Furthermore, the *SRC* pathway score correlates negatively with PKCι immunoscore (Figure 5F) and with PKCι-driven *ECT2* and *MEK* pathway scores (Figures 5G and 5H) across our panel of human GBM PDX samples.

PKCι- and SRC-dependent GBMs exhibit distinct therapeutic vulnerabilities

Our data suggest that PKCι- and SRC-dependent GBM tumors will exhibit differential sensitivities to PKCι and SRC inhibitors. Consistent with this prediction, PKCι-dependent *Trp53*$^{-/-}$ GBM cells are highly sensitive to auranofin (Figure 4A) but relatively insensitive to saracatinib or dasatinib (Figures 6A and 6B), two SRC inhibitors (Hantschel et al., 2008; Hennequin et al., 2006). In contrast, PKCι-independent *Trp53*$^{-/-}$/*Prkci*$^{-/-}$ GBM cells are resistant to auranofin (Figure 4A) but are highly sensitive to both SRC inhibitors (Figures 6A and 6B). To extend our results, we analyzed the same panel of mouse and human GBM cell lines shown in Figures 2A and 2B for sensitivity to SRC inhibition. Interestingly, a plot of saracatinib EC_{50} versus auranofin EC_{50} values in human and mouse GBM cell lines (Table S2) fits a rectangular hyperbola (Figure 6C), indicating that the sensitivities to these two drugs are inversely related. Furthermore, human PDX-derived GBM cell lines expressing high PKCι (and high sensitivity to auranofin; Figure 2F) are relatively resistant to saracatinib when compared with their low PKCι-expressing counterparts (Figure S4C). Thus, there is a reciprocal relationship between auranofin and saracatinib sensitivity in both murine and human GBMs. Although saracatinib and dasatinib inhibit SRC, they can also inhibit other tyrosine kinases. For instance, saracatinib inhibits EGFR, whereas dasatinib does not (Figure S4D). However, the EGFR-specific inhibitor erlotinib has no effect on viability of either *Trp53*$^{-/-}$ or *Trp53*$^{-/-}$/*Prkci*$^{-/-}$ cells, indicating that EGFR is not the relevant target (Figure S4E). Although both saracatinib and dasatinib can also inhibit cABL (Hantschel et al., 2008; Hennequin et al., 2006), *Prkci* deletion has little effect on activating

cABL phosphorylation, suggesting that the effects of these inhibitors are not due to cABL inhibition (Figure S5B).

Reciprocal mechanisms of acquired resistance to PKCι and SRC inhibition

Because GBM cells exhibit an inverse relationship between sensitivity to PKCι and SRC inhibition (Figure 6C), we next investigated the effect of acquired resistance to auranofin and dasatinib on PKCι and SRC signaling. Three auranofin-sensitive/saracatinib-insensitive *Trp53*$^{-/-}$ GBM cell lines (Figures 4A and 6A; Table S2) were made resistant to auranofin by culturing them in increasing concentrations of this drug. The resultant cells exhibited auranofin EC_{50}s that are >10-fold higher than auranofin-naive *Trp53*$^{-/-}$ GBM cells (378–711 nM) (Figure 6D; Table S2), essentially indistinguishable from the auranofin EC_{50} of *Trp53*$^{-/-}$/*Prkci*$^{-/-}$ GBM cells (Table S2). Interestingly, these cells now exhibit sensitivity to saracatinib (Figure 6E) and a >2-fold increase in SRC phosphorylation (Figure 6F). Although RNA-seq data from our *Pten*$^{-/-}$ and *Trp53*$^{-/-}$ models demonstrate that these cells express three SRC family members (*Src*, *Lyn*, and *Fyn*) (Sonabend et al., 2013), only SRC phosphorylation is increased in auranofin-resistant cells (Figure 6F; Figures S4F and S4G), indicating that SRC activation plays a selective role in acquired resistance to auranofin.

We also made two saracatinib-sensitive/auranofin-insensitive (MES1861 and MES4622) murine GBM cell lines (Table S2) resistant to dasatinib by culturing them in increasing concentrations of dasatinib. Dasatinib resistance was associated with increased sensitivity to both auranofin and CRT0066854 (Figures 6G and 6H), an ~2-fold increase in PKCι protein expression (Figure 6I), and an ~3-fold increase in ECT2 and ERK phosphorylation (Figures S5C and S5D), consistent with activation of PKCι signaling in dasatinib-resistant cells.

Human GBMs harbor PKCι-dependent and SRC-dependent tumor cell populations

A hallmark of GBM is intratumoral heterogeneity, as demonstrated by single-cell RNA-seq (scRNA-seq) studies (Neftel et al., 2019; Patel et al., 2014; Yuan et al., 2018). We therefore calculated *ECT2*, *MEK*, and *SRC* pathway scores for 20,088 individual glioma cells that correspond to 39 distinct tumor cell clusters from eight high-grade gliomas for which scRNA-seq data were available (Yuan et al., 2018). Heatmap analysis showed that most tumor cell clusters (28/39) were enriched for at least one of these three pathways. PKCι-related pathways were predominant, with 24 cell clusters enriched in either *ECT2* or *MEK* pathway scores, and 11 enriched in both. In contrast, only six cell clusters were enriched in *SRC* pathway score. Importantly, only two clusters were enriched for both *SRC* and *MEK* pathway scores, and none were enriched for both *SRC* and *ECT2* pathway scores (Figure 7A). Spearman correlation analysis showed that *ECT2* and *MEK* pathway scores are positively correlated with each other ($r = 0.39$ $p = 0.02$), while the *SRC* pathway score is negatively correlated with both *ECT2* ($r = -0.52$, $p = 0.0009$) and *MEK* ($r = -0.29$, $p = 0.07$) pathway scores (Figures 7B–7D). These data are consistent with the reciprocal, inverse relationship we observe between PKCι and SRC signaling pathway activity and inhibitor sensitivity in GBM cell lines. We also assessed the relative abundance of tumor cell populations enriched for *ECT2* or *SRC* pathway scores. Notably, all tumors contain a population of cells exhibiting high ECT2/low SRC pathway scores; in addition, most tumors (5/8) contain an additional population exhibiting low ECT2/high SRC pathway scores,

although these account for a smaller fraction of the total. Furthermore, most tumors (6/8) also contain a cell population exhibiting low ECT2/low SRC pathway scores (Figure 7E). Together, these findings reveal considerable intra-tumoral heterogeneity and demonstrate that most GBM tumors contain distinct sub-populations of cells exhibiting either PKCι or SRC pathway activation. Furthermore, many GBM tumors contain additional cell sub-population(s) without apparent activation of either pathway.

Because GBMs often contain both PKCι- and SRC-dependent cell populations (Figure 7E), and acquired resistance to either PKCι or SRC inhibitors is associated with activation of the uninhibited pathway, we reasoned that combined auranofin and saracatinib therapy might be more effective than either drug alone. To test this hypothesis, mice bearing *Trp53*$^{-/-}$ GBM tumors were treated with auranofin, saracatinib, or the combination and assessed for overall survival. Auranofin significantly prolonged survival compared with vehicle (Figure 7F), consistent with the effect of *Prkci* deletion (Figure 3A). In contrast, survival of mice with *Trp53*$^{-/-}$ tumors is unaffected by saracatinib (Figure 7F), consistent with the fact that *Trp53*$^{-/-}$ GBM cells are saracatinib resistant *in vitro* (Figure 6A). However, combining auranofin with saracatinib significantly prolongs survival beyond that seen with either drug alone (Figure 7F). By contrast, mice harboring *Trp53*$^{-/-}$/*Prkci*$^{-/-}$ GBMs do not respond to auranofin, whereas saracatinib significantly prolonged survival (Figure 7G). To assess the effect of this drug combination in human GBM, we established orthotopic tumors from the human PDX-derived L1 cell line, a tumor-initiating cell (TIC) line that expresses high PKCι levels, is sensitive to auranofin, and is insensitive to saracatinib (Figure 2A; Table S2). Our results demonstrate that these tumors respond to auranofin, but not to saracatinib, and exhibit a significantly enhanced response to combined auranofin and saracatinib beyond the response to auranofin alone (Figure 7H).

DISCUSSION

PKCι is an oncogenic driver in GBM

In this study, we provide two compelling lines of evidence that *PRKCI* is a key oncogenic driver of GBM. First, we show that *PRKCI* CNGs and activated PKCι signaling are associated with progression of LGGs to GBM. These data indicate that *PRKCI* CNG may be a useful biomarker to identify those LGGs likely to progress to GBM. These results are consistent with our findings that *PRKCI* expression and CNGs are strongly associated with malignant progression of preneoplastic bronchial lesions and squamous carcinoma *in situ* to lung squamous cell carcinoma (*LUSC*) (Liu et al., 2020b). We also demonstrated that coordinate overexpression of the three oncogenes on chromosome 3q26, *PRKCI*, *ECT2*, and *SOX2*, is necessary and sufficient to transform lung basal stem cells into LUSC (Liu et al., 2020b). *PRKCI* CNG correlates with poor outcome, and malignant progression in LGGs strongly implicates *PRKCI* as a heretofore unappreciated driver of GBM. Second, we demonstrate in two GEMMs that deletion of the mouse PKCι gene, *Prkci*, slows GBM tumorigenesis and prolongs survival. In both mouse and human GBM, PKCι drives cell proliferation and invasion by activating oncogenic PKCι-ECT2 and MEK-ERK signaling.

Transformed growth and invasion are key features of GBM, and inhibiting one often stimulates the other (Dhruv et al., 2013; Lu et al., 2012; Picariello et al., 2019), suggesting

that effective therapy for GBM needs to inhibit both. Acute treatment with auranofin, an FDA-approved, BBB-permeant small-molecule inhibitor of PKCι (Madeira et al., 2013), inhibits growth and invasion in GBM cells *in vitro* and *in vivo*. The fact that GBMs can arise despite genetic deletion of *Prkci* in mouse glial progenitor cells indicates that compensatory pathways can overcome *Prkci* loss over time. Our data clearly demonstrate that at least one of these is driven by *SRC*. Importantly, sensitivity to two PKCι inhibitors (*auranofin*, *CRT0066854*) correlates with PKCι expression, demonstrating that growth inhibition by auranofin is due to PKCι inhibition. These data provide compelling evidence that PKCι is a relevant therapeutic target for GBM, and that PKCι expression profiling may be useful in predicting responsiveness to PKCι-directed therapy. Invasion and self-renewal are also defining features of TICs, and we have shown that in KRAS-driven lung adenocarcinoma (LUAD), PKCι drives a TIC phenotype through its control of NOTCH3 signaling (Ali et al., 2016). A PKCι-NOTCH signaling axis has been found to be necessary for glioma TIC survival (Phillips et al., 2016). Whether PKCι inhibition in GBM suppresses a TIC phenotype will be the subject of further investigations in our laboratories.

PKCι and SRC signaling are reciprocally related in GBM

That lethal GBMs still develop with *Prkci* deletion or PKCι inhibition demonstrates that GBMs can activate alternative oncogenic pathways to maintain tumor growth and survival. Using the TCGA GBM dataset, we found that low *PRKCI*-expressing GBMs activate SRC signaling, while high *PRKCI*-expressing GBMs do not. We validated the reciprocal nature of PKCι and SRC signaling activity using an independent transcriptomic dataset from PDX-derived GBM models. Elevated *PRKCI* expression is positively associated with active PKCι-ECT2 and MEK-ERK signaling and negatively associated with active SRC signaling. We also observed a reciprocal relationship between PKCι and SRC signaling in our *Prkci* KO murine GBM cell lines, which exhibit increased SRC activation. Furthermore, auranofin-resistant murine GBM cell lines activate SRC signaling and show increased sensitivity to a SRC inhibitor, while dasatinib-resistant lines increase both PKCι signaling and sensitivity to auranofin. Thus, not only are PKCι and SRC signaling pathways inversely related, activation of one pathway provides resistance to inhibitors of the other. Acutely targeting PKCι *in vitro* with auranofin is highly toxic to PKCι high-expressing tumor cells and inhibits *in vitro* invasion. By contrast, tumor cells derived from murine *Trp53*$^{-/-}$/*Prkci*$^{-/-}$ GBMs (Figure 3A) are less impaired in proliferation and invasion (Figures 3E and 3F). This implies that the capability of Src to rescue cells deprived of PKCι function develops over time, so that *Prkci*-deleted tumors eventually grow, invade, and ultimately kill their hosts (Figure 3A). However, the fact that Src activation does not completely restore proliferation and invasion in *Prkci*-deleted tumors also suggests that there may be a hierarchy of signaling kinases with some, such as PKCι, more effective than others, such as Src, in driving the malignant phenotype in GBM.

This reciprocity between PKCι and other oncogenic signaling drivers may apply to other malignancies as well. For example, we recently demonstrated that murine LUAD tumors can be divided into genomically distinct, reciprocally related subtypes based on *PRKCI* CNG and PKCι expression (Liu et al., 2020a, 2020b; Yin et al., 2019, 2020). However, in this case, PKCι-independent LUADs activate WNT signaling and are sensitive to WNT

pathway inhibitors. Analysis of scRNA-seq data revealed no enrichment in a WNT pathway signature in any GBM cell populations (data not shown), suggesting that WNT may not have a major role in PKCι-independent signaling in GBM. Our current data also establish that SRC activation provides a mechanism of resistance to auranofin in GBM. Whether WNT pathway activation provides a similar mechanism in LUAD remains to be determined.

GBMs contain three distinct tumor cell populations distinguished by their relative dependencies on PKCι and SRC

Data from bulk transcriptomics include contributions from both tumor and stromal cells, the latter of which can constitute up to 50% of a GBM (Chen et al., 2017). We therefore turned to a scRNA-seq dataset, which confirmed the reciprocal relationship between PKCι and SRC signaling across tumor cell clusters. This work revealed that nearly all GBM tumors contain a mixture of high PKCι/low SRC and low PKCι/high SRC cell subpopulations, but no high ECT2/high SRC cells and only rare high MEK/high SRC cells (Figures 7A–7E). However, this analysis also revealed that approximately 30% of cell clusters are characterized by low activity in both PKCι and SRC pathways. Our results are consistent with the intratumoral heterogeneity that characterizes GBMs (Neftel et al., 2019; Patel et al., 2014; Yuan et al., 2018) and demonstrate that the proportion of tumor cell clusters in these three subpopulations varies considerably from tumor to tumor. The presence of three distinct tumor cell populations likely explains why pharmacologically targeting either PKCι or SRC eventually fails, because suppression of one subgroup would lead to clonal expansion of the other two, a mechanism that may also explain why dasatinib has been ineffective in clinical trials in GBM (Galanis et al., 2019; Lassman et al., 2015). Although combining auranofin with saracatinib would be expected to prolong survival over either drug alone (Figures 7F and 7H), this combination would also select for clonal expansion of the third, low PKCι/low SRC tumor cell population, leading to eventual tumor progression and mortality. Further studies will be needed to identify and functionally characterize the oncogenic pathway(s) that drives proliferation of this third cell population. Such pathways could represent therapeutic vulnerabilities that could further improve our combination therapy approach.

Defining a translationally actionable GBM classification scheme

Multiple investigations have used “omic” analyses to develop classification schemes for GBM (Neftel et al., 2019; Patel et al., 2014; Verhaak et al., 2010; Wang et al., 2021; Yuan et al., 2018). These schemes have provided important insights into functional differences between GBM tumors and the cell populations that comprise them. In many cases, the subgroups identified by these studies have been linked to amplified or mutated oncogenic signaling pathways. However, with one exception (Wang et al., 2020), none of these studies have shown that targeting these pathways produces a therapeutic response in GBM, nor have any examined how resistance to these targeted therapies develops. Such resistance has been attributed to the high degree of cellular heterogeneity in these tumors (Neftel et al., 2019; Patel et al., 2014; Wang et al., 2020; Yuan et al., 2018). It has been proposed that addressing this problem will require the use of drug combinations (Al-Lazikani et al., 2012), although the complex composition of cell populations that make up GBM has made the prospect of identifying such combinations daunting. By contrast, we have used a

different approach that is based upon four principles. The first is that although GBMs are highly heterogeneous, the multiple subpopulations that comprise them can nonetheless be consolidated into a small number of groups, each defined by a dependency upon a distinct oncogenic driver. The second is that resistance to one targeted therapy is due to outgrowth of an intrinsically resistant subpopulation that depends on a different signaling pathway. The third is that determining how tumors develop resistance to a drug will yield insights into how to target the resistant population. Finally, the fourth is that targeting multiple subpopulations in a tumor with combination therapy can delay recurrence without dose-limiting toxicities. Our study of PKCι and SRC signaling and inhibition confirms the validity of our therapeutic approach. We anticipate that the principles underlying this work will lead to the development of additional targeted therapy combinations to both treat GBM and slow or prevent the emergence of resistance.

Limitations of the study

Our study has focused on a reciprocal relationship between PKCι and SRC, which has allowed us to characterize subpopulations of tumor cells in both human and murine GBMs. Our results do not exclude the possibility that reciprocal relationships with other pairs of GBM-relevant oncogenic kinases may also exist, or that other classification schemes could be constructed that also are based on these pathways. Nevertheless, our ability to significantly improve survival in GBM models with combined inhibition of both PKCι and SRC speaks to the translational importance of this current study. A second limitation relates to the dose-response studies of SRC and PKCι inhibitors. These *in vitro* studies on tissue culture surfaces do not recapitulate the cellular or mechanical features of the microenvironments that characterize a GBM. Although predictions made from these *in vitro* experiments are consistent with *in vivo* studies of PKCι and SRC inhibitors in murine GBM models, it remains possible that local variations in microenvironment from tumor to tumor, as well as genetic drift that can occur in some culture conditions, may ultimately impact the efficacy of combined PKCι and SRC targeting. Assessing this issue will require larger-scale studies using multiple PDX models and/or *ex vivo* brain slice studies of drug sensitivity, and results of such studies will be needed before our findings can be translated into clinical therapy.

STAR★METHODS

RESOURCE AVAILABILITY

Lead contact—Further information and requests for resources and reagents should be directed to and will be fulfilled by the lead contact, Steven S. Rosenfeld (rosenfeld.steven@mayo.edu).

Materials availability—Genetically engineered mouse models and cell lines will be distributed after completion of the relevant Materials Transfer Agreements with the Mayo Clinic.

Data and code availability

- The single cell RNA-seq data used in this study are publicly available on the Gene Expression Omnibus under accession GSE103224. The bulk RNA-seq data derived from human glioblastoma tissue microarrays are publicly available through the cBioPortal for Cancer Genomics. Accession information is available in the Key resources table. All other data reported in this paper will be shared by the lead contact upon request.
- This paper does not report any original code.
- Any additional information required to reanalyze the data is available from the lead contact upon request.

EXPERIMENTAL MODEL AND SUBJECT DETAILS

Mice—All mouse procedures were performed in compliance with the Mayo Clinic Institutional Animal Care and Use Committee guidelines (protocol numbers A00002923 and A00004179). Homozygous floxed *Pten* mice (Stock #006440), floxed *Trp53* mice (Stock #008462) and NOD-SCID mice (Stock #005557) were obtained from Jackson Laboratory. Previously described floxed *Prkci* (*Prkci*$^{fl/fl}$) mice (Regala et al., 2009; Yin et al., 2019) were crossed with *Pten53*$^{fl/fl}$ and *Trp53*$^{fl/fl}$ mice to generate *Pten53*$^{fl/fl}$/*Prkci*$^{fl/fl}$ mice and *Trp53*$^{fl/fl}$/*Prkci*$^{fl/fl}$ mice. Studies were performed on equal numbers of male and female mice between. 7–12 weeks of age.

Human GBM tissue microarrays—Information on the human PDX lines used to constitute the tissue microarrays is provided in Table S4. This information is also available through the following publicly available database: https://www.mayo.edu/research/labs/translational-neuro-oncology/mayo-clinic-brain-tumor-patient-derived-xenograft-national-resource/overview. Tissue for microarrays was obtained under protocol numbers 11–006108 and 07–007623 approved by the Mayo Clinic Institutional Review Board

Glioma cell line isolation from mouse GBM tumor and culture—The protocol for primary tumor isolation has been described (Lei et al., 2011). Primary glioma cells were grown on tissue culture plates coated with 10μg/mL Fibronectin (Millipore). To generate auranofin-resistant GBM cells, *Trp53*$^{-/-}$ GBM cells were cultured in the presence of 50 nM auranofin for first week, 100 nM for the second week, and 150 nM for the third week, and then maintained in the presence of 150 nM of auranofin. Murine mesenchymal (MES) glioblastoma cells (MES1861 and MES4622) which lack expression of *Nf1* and *Trp53* were maintained in DMEM media with 10% FBS as previously described (Gürsel et al., 2011; Reilly et al., 2000), while mouse proneural (PN) glioblastoma cells PN20, PN24, PN62 were derived from primary PDGFB-driven glioblastomas generated in *Nestin-tva:Cdkn2A* knockout mice (Hambardzumyan et al., 2009) and grown in mouse neural stem cell medium (STEMCELL Technologies, 05700 and 05701), supplemented with 20 ng/ml hEGF (Sigma-Aldrich, E9644), 10 ng/ml hFGF (R&D systems, 233-FB-025) and 2 μg/ml heparin (STEMCELL Technologies, 07980). Dasatinib-resistant MES glioblastoma cells were generated by culturing in the presence of 500 nM dasatinib for first week, 750 nM for

the second week, and 1000 nM for the third week, and then maintained in the presence of 1000 nM of dasatinib.

Human L0 and L1 GBM cells were cultured and maintained in DMEM+F12 media with 1% N2 supplement (GIBCO), 20ng/ml of hEGF (Sigma-Aldrich) and 20ng/ml of hFGF (R&D systems). Human GBM cells 1A, 108, 120, 612, 1171 and 651 were cultured and maintained in DMEM+F12 media with 1% NeuroPlex supplement (Gemini), 20ng/ml of EGF and 20ng/ml of FGF. Human GBM cell lines 8, 43, 12, and 10 were obtained from the Mayo Clinic Brain Tumor PDX National Resource.

METHOD DETAILS

Western blot analysis—Cells were incubated in lysis buffer (50 mM Tris HCl at pH 7.40, 150 mM NaCl, 1 mM EDTA, 1.0% Nonidet P-40, and a mixture of protease and phosphatase inhibitors), debris was removed by centrifugation for 10 mins at high speed at 4°C, and cleared lysates were run on SDS/PAGE and transferred to PVD membranes. Membranes were blocked in 5% non-fat dry milk in TBS + 0.1% Tween 20 for 1 hour, incubated with primary antibody in blocking solution for 2 hours, followed by secondary antibody for 1 hour at room temperature, and developed using enhanced chemiluminescence solution.

Transwell *in vitro* invasion assays—Fluoroblok Transwell inserts were coated with 5 μg/ml laminin for 1 hour at 37°C, then washed with PBS before adding 125,000 cells for each insert. 10% FBS was used as a chemoattractant. Cells were incubated for 15 hours at 37°C, inserts were washed with PBS, fixed in 4% PFA for 15 min and washed twice with PBS before staining with DAPI. Images were captured and analyzed for nuclear count using Cytation 5.

Proliferation assays—1000 cells/well were plated in 96-well plates, the plates were scanned and phase-contrast images (4 per well) were acquired every 12 hours for 6 days using Cytation 5.

Cell viability assays—5000 cells/well were plated in 96-well plates and allowed to attach for 48 hours. Cells were treated with auranofin (Santa Cruz Biotechnology, cat# SC202476A), CRT0066854 (Tocris, cat# 5922), saracatinib (Selleck Chemicals, cat# S1006), dasatinib (Selleck Chemicals, cat# S1021), or erlotinib (Selleck Chemicals, cat# S7786) for 72 hours. Cell viability was determined using CellTiter-Glo and results normalized to cells treated with vehicle.

RAC1 activity assays—RAC1 activity was assessed by affinity pull-down of GTP-bound RAC1 using binding domains of PAK, as previously described (Justilien and Fields, 2009).

Retrovirus production and intracerebral injections—The PDGF-IRES-cre retrovirus was generated and injected intracranially according to methods described previously (Kenchappa et al., 2020; Lei et al., 2011). For the pharmacologic studies mice were treated five days after retroviral injection with vehicle, saracatinib (*17.5 mg/kg by oral gavage, 5 days per week*), auranofin (*12 mg/kg by intraperitoneal injection, 6 days*

per week), or auranofin + saracatinib (*12 mg/kg by intraperitoneal injection 6 days/week; 17.5 mg/kg by oral gavage 5 days/week, respectively*) with 7–8 mice per treatment group. Treatment continued until tumor morbidity. For studies using the L1 GBM PDX model, NOD/SCID mice were orthotopically injected with 100,000 human L1 GBM cells (kindly provided by Dr. Justin Lathia, Cleveland Clinic), and treatment with vehicle, auranofin, and/or saracatinib began 20 days later.

Brain histological analysis—Brains from 4% paraformaldehyde-perfused, GBM-bearing mice were paraffin-embedded as described (Kenchappa et al., 2020). IHC was performed on 5 μm sections using the Discovery ULTRA automated stainer (Ventana Medical Systems). Antigen retrieval was performed using a Tris/borate/EDTA buffer (Discovery CC1), pH 8.0–8.5, for 60 minutes at 95°C. Slides were incubated with anti-Ki67 for 2 hours at room temperature. The antibodies were visualized using biotinylated goat anti-rabbit and rabbit anti-rat secondary and counterstained with hematoxylin and eosin (H&E). Images were captured and analyzed using a ScanScope scanner and ImageScope software (Aperio Technologies).

Analysis of Tissue Microarrays (TMAs)—GBM patient tumor samples were collected following informed consent under a protocol approved by the Mayo Clinic Institutional Review Board (protocol #12–003458). TMAs were built from formalin-fixed, paraffin-embedded blocks from 68 de-identified GBM patient tumor samples using between 3–6 independent cores from each patient sample. The TMA slides were baked, deparaffinized for 15 min in xylene, rehydrated using graded alcohols and washed with distilled water, and then treated with antigen retrieval solution (pH 9.0, Dako) for 25 min at 100°C. Slides were washed in tap water followed by wash buffer (Dako) and then treated with 3% hydrogen peroxide for 5 minutes followed by serum-free protein block (Dako) for 5 min. PKCι (1:1600, BD Biosciences, cat #610176) and Ki67 (1:1000 for Ki67, Vector Laboratories, cat# VP-K451) antibodies were diluted and incubated for 60 minutes at room temperature. Slides were washed twice with wash buffer, incubated with anti-mouse labeled polymer for 30 min at room temperature, washed twice in wash buffer, and incubated with DAB for 5 min at room temperature and rinsed in distilled water. The slides were counterstained in hematoxylin, dehydrated and mounted. TMAs stained for PKCι and Ki67 were scanned at 20x magnification using an Aperio AT2 slide scanner (Leica Biosystems) and images were visualized using Aperio Slide Imaging software. PKCι and Ki67 staining analysis was performed using the Aperio ScanScope ™ software. Regions of interest containing tumor tissue were selected in each case. The software is designed to apply a positive pixel algorithm to each ROI, and the resulting number of positive pixels is divided by the total number of pixels to generate an immunoscore, ranging from 0–1.

QUANTIFICATION AND STATISTICAL ANALYSIS

Statistical analysis—For *in vitro* studies, a two tailed t test or one-way ANOVA was used to calculate p values with statistical significance at $p < 0.05$. Individual experimental values were independent of each other and could be fit to a normal distribution. For survival studies, statistical significance was determined using a log rank test, and significance was set at $p < 0.05$. None of the data was censored. The analysis of percentile *PRKCI* copy number

alterations across different molecular subtypes was performed using the chi-square test. When comparing groups a one-way ANOVA statistical test was used applying the Dunnett's method or Tukey's method to correct for multiple comparisons. Statistical analysis was performed using the computing environment R. For each experiment, the type of statistical test used is indicated in relevant sections of the text and in the **Figure Legend**.

Data accession and pre-processing—Primary Glioblastoma (GBM) tumors and Low Grade Glioma (LGG) tumor data was downloaded from The Cancer Genome Atlas (TCGA) data portal (https://www.cbioportal.org/). Tumors from 1,107 patients were assayed on at least one molecular profiling platform, which included: (1) RNA sequencing; (2) DNA copy-number assay, (3) gene expression Affymetrix HT-HGU133A array. RNA-seq data from 156 primary GBM tumors and 513 LGG tumors and gene expression microarray data from 529 GBM tumors were analyzed to identify the role of PKCι pathway activation and copy number alteration in diffuse gliomas. Dataset GSE57872 was downloaded from the NCBI Gene Expression Omnibus (GEO) database to identify GBM classification and PKCι-ECT2, MEK and SRC pathway scores across 3 GBM subtypes. A second dataset of 42 GBMs from the GBM TMAs (obtained from the Mayo Clinic Brain Tumor Patient Derived Xenograft National Resource) for which RNA-seq data was available was analyzed as described above.

Fitting of dose response data and of the variation of EC_{50} with auranofin and CRT0066854 was performed using Prism 9 (GraphPad). For dose response curves in Figures 4A and 4C, fitting was constrained to include data between 5% and 95% of the maximum drug concentration used.

Single-cell RNA sequencing data of eight tumors from patients with high grade glioma from Yuan et al., 2018 was used for the analysis. Transcript-level count data was downloaded from GEO accession GSE103224 (Yuan et al., 2018).

Gene Set Enrichment Analysis (GSEA)—The Gene Set Enrichment Analysis (GSEA) software is publicly available from the Broad Institute of MIT and Harvard University (https://www.gsea-msigdb.org/gsea/index.jsp). RPKM-normalized gene counts from TCGA primary tumors and PDX models were downloaded to GSEA software for Hallmark, KEGG, and Oncogenic Signature analysis (version h.all.v7). Analysis of differentially enriched Hallmarks, KEGG pathways, and Oncogenic Signatures (*Top25* versus *Btm25*) in TCGA primary tumors were performed separately. GSEA was performed using the gene permutation option and gene sets smaller than 15 or larger than 500 were excluded. The false discovery rate (FDR) of hallmark with less than 0.25 (FDR < 0.25) was considered as significant enriched.

Marker selection, clustering, and visualization—Marker selection, UMAP projections, clustering, and cluster-specific differential expression for each tumor was performed using the computational pipeline described in (Mizrak et al., 2019; Yuan et al., 2018) (https://github.com/simslab/cluster_diffex2018). Verhaak tumor subtypes for each patient were defined, and cell populations were annotated by cell type (with transformed cells defined by copy number variations) as described in (Yuan et al., 2018). Data was then

loaded into programming language R via the Seurat package 4.0.1 for downstream analysis and visualization.

Pathway Score Analysis of GBMs and LGGs—PKCι-ECT2 pathway signature genes consist of the 12 ribosomal RNA processing genes that most highly correlate with *PRKCI* and *ECT2* expression in the TCGA GBM dataset. PKCι-MEK pathway signature genes consists of 13 MAPK_SIGNALING_PATHWAY genes differentially expressed in the Top25 versus the Btm25 *PRKCI* expression groups in the TCGA GBM dataset, and whose expression drives the association between high *PRKCI* expression and MAPK pathway activation (leading edge genes). SRC pathway signature genes consists of SRC_UP.V1_UP genes differentially expressed in the Top25 versus the Btm25 *PRKCI* expression groups in the TCGA GBM dataset, and whose expression drives the association between low *PRKCI* expression and SRC pathway activation (leading edge genes). Signature genes in each group, fold change, and p values are indicated in Table S1. The pathway score represents the principal component analysis (PCA) of the expression matrix of ECT2, MEK and SRC signature genes and positively correlates with mean expression of those genes. The pathway score can be applied using the built-in R prcomp and princomp functions.

For scRNaseq analysis, Cluster-specific differential expression analysis was used for each cluster to rank genes by log2-fold change and perform Pre-ranked Gene Set Enrichment Analysis on the three signatures described above (PKCι-ECT2, PKCι-MEK, and SRC) for each patient-specific cluster to generate Normalized Enrichment Scores (NES) (Subramanian et al., 2005). NES were then projected on patient-specific UMAP projections. Tumor clusters across all patients were isolated and the NES for each cluster were visualized in a heatmap, with hierarchical clustering performed with correlation as the distance measure, using the R Bioconductor package ComplexHeatmap (Gu). Spearman correlation (including Spearman's rank correlation test) was performed across all patient tumor clusters comparing NES of the PKCι-ECT2, PKCι-MEK, and SRC signatures, and scatterplots were generated comparing cluster enrichment of PKCι and SRC signatures. Each tumor cluster for each patient was then defined as either High PKCι (PKCι-ECT2 NES > 0) or Low PKC (PKCι-ECT2 NES < 0) and either High SRC (SRC NES > 0) or Low SRC (SRC NES < 0). Chi-square test was performed to assess relationship between Verhaak subtype and PKCι/SRC identity across all tumor clusters.

Supplementary Material

Refer to Web version on PubMed Central for supplementary material.

ACKNOWLEDGMENTS

S.S.R. was supported by NIH grants R01NS073610, R01NS118513, R61NS119714, and U54CA210910 and by a Translational Adult Glioma Award from the Ben and Catherine Ivy Foundation. A.P.F. was supported by NIH grants R01CA081436 and R01CA206367, by a Translational Adult Glioma Award from the Ben and Catherine Ivy Foundation, and by the Monica Flynn Jacoby Professorship. A.Q.-H. was supported by NIH grants R01CA200399, R01CA195503, and R01CA216855. R.S.K. was supported by grant SUB00002520 from the Florida Center for Brain Tumor Research and NIH grant R01NS118513. P.C. was supported by NIH grants R01NS073610 and R01NS118513. Y.L. was supported by an Edward C. Kendall Fellowship in Biochemistry from the Mayo Clinic. D.H. was supported by NIH grants R01NS100864 and R21NS106554. V.J. was supported by grant RSG-18–201-01 from the American Cancer Society. J.N.S. was supported by NIH grants U54 CA210180 and U01CA227954 and

by a Translational Adult Glioma Award from the Ben and Catherine Ivy Foundation. We wish to thank Dr. Justin D. Lathia (Lerner Research Institute of the Cleveland Clinic Foundation) for his gift of L0 and L1 cells, Brandy Edenfield (Mayo Clinic Histology Facility) for excellent technical assistance, and Trine Gaever for the graphical abstract and Figure 4A.

REFERENCES

Al-Lazikani B, Banerji U, and Workman P (2012). Combinatorial drug therapy for cancer in the post-genomic era. Nat. Biotechnol 30, 679–692. [PubMed: 22781697]

Ali SA, Justilien V, Jamieson L, Murray NR, and Fields AP (2016). Protein Kinase Cι Drives a NOTCH3-dependent Stem-like Phenotype in Mutant KRAS Lung Adenocarcinoma. Cancer Cell 29, 367–378. [PubMed: 26977885]

Baldwin RM, Parolin DA, and Lorimer IA (2008). Regulation of glioblastoma cell invasion by PKC iota and RhoB. Oncogene 27, 3587–3595. [PubMed: 18212741]

Ceccarelli M, Barthel FP, Malta TM, Sabedot TS, Salama SR, Murray BA, Morozova O, Newton Y, Radenbaugh A, Pagnotta SM, et al. ; TCGA Research Network (2016). Molecular Profiling Reveals Biologically Discrete Subsets and Pathways of Progression in Diffuse Glioma. Cell 164, 550–563. [PubMed: 26824661]

Chen Z, Feng X, Herting CJ, Garcia VA, Nie K, Pong WW, Rasmussen R, Dwivedi B, Seby S, Wolf SA, et al. (2017). Cellular and Molecular Identity of Tumor-Associated Macrophages in Glioblastoma. Cancer Res. 77, 2266–2278. [PubMed: 28235764]

De Witt Hamer PC (2010). Small molecule kinase inhibitors in glioblastoma: a systematic review of clinical studies. Neuro-oncol. 12, 304–316. [PubMed: 20167819]

Deleyrolle LP, Harding A, Cato K, Siebzehnrubl FA, Rahman M, Azari H, Olson S, Gabrielli B, Osborne G, Vescovi A, and Reynolds BA (2011). Evidence for label-retaining tumour-initiating cells in human glioblastoma. Brain 134, 1331–1343. [PubMed: 21515906]

Desai S, Pillai P, Win-Piazza H, and Acevedo-Duncan M (2011). PKC-ι promotes glioblastoma cell survival by phosphorylating and inhibiting BAD through a phosphatidylinositol 3-kinase pathway. Biochim. Biophys. Acta 1813, 1190–1197. [PubMed: 21419810]

Desai SR, Pillai PP, Patel RS, McCray AN, Win-Piazza HY, and Acevedo-Duncan ME (2012). Regulation of Cdk7 activity through a phosphatidylinositol (3)-kinase/PKC-ι-mediated signaling cascade in glioblastoma. Carcinogenesis 33, 10–19. [PubMed: 22021906]

Dhruv HD, McDonough Winslow WS, Armstrong B, Tuncali S, Eschbacher J, Kislin K, Loftus JC, Tran NL, and Berens ME (2013). Reciprocal activation of transcription factors underlies the dichotomy between proliferation and invasion of glioma cells. PLoS ONE 8, e72134. [PubMed: 23967279]

Dong M, Xiao Q, Hu J, Cheng F, Zhang P, Zong W, Tang Q, Li X, Mao F, He Y, et al. (2020). Targeting LRIG2 overcomes resistance to EGFR inhibitor in glioblastoma by modulating GAS6/AXL/SRC signaling. Cancer Gene Ther. 27, 878–897. [PubMed: 31988476]

Erdogan E, Lamark T, Stallings-Mann M, Lee Jamieson, Pellecchia M, Thompson EA, Johansen T, and Fields AP (2006). Aurothiomalate inhibits transformed growth by targeting the PB1 domain of protein kinase Ciota. J. Biol. Chem 281, 28450–28459. [PubMed: 16861740]

Frederick LA, Matthews JA, Jamieson L, Justilien V, Thompson EA, Radisky DC, and Fields AP (2008). Matrix metalloproteinase-10 is a critical effector of protein kinase Ciota-Par6alpha-mediated lung cancer. Oncogene 27, 4841–4853. [PubMed: 18427549]

Galanis E, Anderson SK, Twohy EL, Carrero XW, Dixon JG, Tran DD, Jeyapalan SA, Anderson DM, Kaufmann TJ, Feathers RW, et al. (2019). A phase 1 and randomized, placebo-controlled phase 2 trial of bevacizumab plus dasatinib in patients with recurrent glioblastoma: Alliance/North Central Cancer Treatment Group N0872. Cancer 125, 3790–3800. [PubMed: 31290996]

Galli R, Binda E, Orfanelli U, Cipelletti B, Gritti A, De Vitis S, Fiocco R, Foroni C, Dimeco F, and Vescovi A (2004). Isolation and characterization of tumorigenic, stem-like neural precursors from human glioblastoma. Cancer Res. 64, 7011–7021. [PubMed: 15466194]

Gürsel DB, Connell-Albert YS, Tuskan RG, Anastassiadis T, Walrath JC, Hawes JJ, Amlin-Van Schaick JC, and Reilly KM (2011). Control of proliferation in astrocytoma cells by the receptor

tyrosine kinase/PI3K/AKT signaling axis and the use of PI-103 and TCN as potential anti-astrocytoma therapies. Neuro-oncol. 13, 610–621. [PubMed: 21636709]

Hambardzumyan D, Amankulor NM, Helmy KY, Becher OJ, and Holland EC (2009). Modeling Adult Gliomas Using RCAS/t-va Technology. Transl. Oncol 2, 89–95. [PubMed: 19412424]

Hantschel O, Rix U, and Superti-Furga G (2008). Target spectrum of the BCR-ABL inhibitors imatinib, nilotinib and dasatinib. Leuk. Lymphoma 49, 615–619. [PubMed: 18398720]

Hennequin LF, Allen J, Breed J, Curwen J, Fennell M, Green TP, Lambert-van der Brempt C, Morgentin R, Norman RA, Olivier A, et al. (2006). N-(5-chloro-1,3-benzodioxol-4-yl)-7-[2-(4-methylpiperazin-1-yl)ethoxy]-5- (tetrahydro-2H-pyran-4-yloxy)quinazolin-4-amine, a novel, highly selective, orally available, dual-specific c-Src/Abl kinase inhibitor. J. Med. Chem 49, 6465–6488. [PubMed: 17064066]

Jatoi A, Radecki Breitkopf C, Foster NR, Block MS, Grudem M, Wahner Hendrickson A, Carlson RE, Barrette B, Karlin N, and Fields AP (2015). A mixed-methods feasibility trial of protein kinase C iota inhibition with auranofin in asymptomatic ovarian cancer patients. Oncology 88, 208–213. [PubMed: 25502607]

Justilien V, and Fields AP (2009). Ect2 links the PKCiota-Par6alpha complex to Rac1 activation and cellular transformation. Oncogene 28, 3597–3607. [PubMed: 19617897]

Justilien V, Jameison L, Der CJ, Rossman KL, and Fields AP (2011). Oncogenic activity of Ect2 is regulated through protein kinase C iota-mediated phosphorylation. J. Biol. Chem 286, 8149–8157. [PubMed: 21189248]

Justilien V, Walsh MP, Ali SA, Thompson EA, Murray NR, and Fields AP (2014). The PRKCI and SOX2 oncogenes are coamplified and cooperate to activate Hedgehog signaling in lung squamous cell carcinoma. Cancer Cell 25, 139–151. [PubMed: 24525231]

Justilien V, Ali SA, Jamieson L, Yin N, Cox AD, Der CJ, Murray NR, and Fields AP (2017a). Ect2-Dependent rRNA Synthesis Is Required for KRAS-TRP53-Driven Lung Adenocarcinoma. Cancer Cell 31, 256–269. [PubMed: 28110998]

Justilien V, Lewis KC, Murray NR, and Fields AP (2017b). Oncogenic Ect2 signaling regulates rRNA synthesis in NSCLC. Small GTPases 10, 388–394. [PubMed: 28657426]

Kenchappa RS, Mistriotis P, Wisniewski E, Bhattacharya S, Kulkarni T, West R, Luu A, Conlon M, Heimsath E, Crish JF, et al. (2020). Myosin 10 Regulates Invasion, Mitosis, and Metabolic Signaling in Glioblastoma. iScience 23, 101802. [PubMed: 33299973]

Kjær S, Linch M, Purkiss A, Kostelecky B, Knowles PP, Rosse C, Riou P, Soudy C, Kaye S, Patel B, et al. (2013). Adenosine-binding motif mimicry and cellular effects of a thieno[2,3-d]pyrimidine-based chemical inhibitor of atypical protein kinase C isoenzymes. Biochem. J. 451, 329–342. [PubMed: 23418854]

Lassman AB, Pugh SL, Gilbert MR, Aldape KD, Geinoz S, Beumer JH, Christner SM, Komaki R, DeAngelis LM, Gaur R, et al. (2015). Phase 2 trial of dasatinib in target-selected patients with recurrent glioblastoma (RTOG 0627). Neuro-oncol. 17, 992–998. [PubMed: 25758746]

Lei L, Sonabend AM, Guarnieri P, Soderquist C, Ludwig T, Rosenfeld S, Bruce JN, and Canoll P (2011). Glioblastoma models reveal the connection between adult glial progenitors and the proneural phenotype. PLoS ONE 6, e20041. [PubMed: 21625383]

Liu Y, Justilien V, Fields AP, and Murray NR (2020a). Recurrent copy number gains drive PKCι expression and PKCι-dependent oncogenic signaling in human cancers. Adv. Biol. Regul 78, 100754. [PubMed: 32992230]

Liu Y, Yin N, Wang X, Khoor A, Sambandam V, Ghosh AB, Fields ZA, Murray NR, Justilien V, and Fields AP (2020b). Chromosome 3q26 Gain Is an Early Event Driving Coordinated Overexpression of the PRKCI, SOX2, and ECT2 Oncogenes in Lung Squamous Cell Carcinoma. Cell Rep. 30, 771–782.e6. [PubMed: 31968252]

Lu KV, Chang JP, Parachoniak CA, Pandika MM, Aghi MK, Meyronet D, Isachenko N, Fouse SD, Phillips JJ, Cheresh DA, et al. (2012). VEGF inhibits tumor cell invasion and mesenchymal transition through a MET/VEGFR2 complex. Cancer Cell 22, 21–35. [PubMed: 22789536]

Madeira JM, Renschler CJ, Mueller B, Hashioka S, Gibson DL, and Klegeris A (2013). Novel protective properties of auranofin: inhibition of human astrocyte cytotoxic secretions and direct neuroprotection. Life Sci. 92, 1072–1080. [PubMed: 23624233]

Mansfield AS, Fields AP, Jatoi A, Qi Y, Adjei AA, Erlichman C, and Molina JR (2013). Phase I dose escalation study of the PKCι inhibitor aurothiomalate for advanced non-small-cell lung cancer, ovarian cancer, and pancreatic cancer. Anticancer Drugs 24, 1079–1083. [PubMed: 23962904]

Mizrak D, Levitin HM, Delgado AC, Crotet V, Yuan J, Chaker Z, Silva-Vargas V, Sims PA, and Doetsch F (2019). Single-Cell Analysis of Regional Differences in Adult V-SVZ Neural Stem Cell Lineages. Cell Rep. 26, 394–406.e5. [PubMed: 30625322]

Neftel C, Laffy J, Filbin MG, Hara T, Shore ME, Rahme GJ, Richman AR, Silverbush D, Shaw ML, Hebert CM, et al. (2019). An Integrative Model of Cellular States, Plasticity, and Genetics for Glioblastoma. Cell 178, 835–849.e21. [PubMed: 31327527]

Olmez I, Zhang Y, Manigat L, Benamar M, Brenneman B, Nakano I, Godlewski J, Bronisz A, Lee J, Abbas T, et al. (2018). Combined c-Met/Trk Inhibition Overcomes Resistance to CDK4/6 Inhibitors in Glioblastoma. Cancer Res. 78, 4360–4369. [PubMed: 29844123]

Parker PJ, Justilien V, Riou P, Linch M, and Fields AP (2014). Atypical protein kinase Cι as a human oncogene and therapeutic target. Biochem. Pharmacol 88, 1–11. [PubMed: 24231509]

Patel AP, Tirosh I, Trombetta JJ, Shalek AK, Gillespie SM, Wakimoto H, Cahill DP, Nahed BV, Curry WT, Martuza RL, et al. (2014). Single-cell RNA-seq highlights intratumoral heterogeneity in primary glioblastoma. Science 344, 1396–1401. [PubMed: 24925914]

Phillips E, Lang V, Bohlen J, Bethke F, Puccio L, Tichy D, Herold-Mende C, Hielscher T, Lichter P, and Goidts V (2016). Targeting atypical protein kinase C iota reduces viability in glioblastoma stem-like cells via a notch signaling mechanism. Int. J. Cancer 139, 1776–1787. [PubMed: 27299852]

Picariello HS, Kenchappa RS, Rai V, Crish JF, Dovas A, Pogoda K, McMahon M, Bell ES, Chandrasekharan U, Luu A, et al. (2019). Myosin IIA suppresses glioblastoma development in a mechanically sensitive manner. Proc. Natl. Acad. Sci. USA 116, 15550–15559. [PubMed: 31235578]

Puduvalli VK, and Hoang N (2018). Chemotherapy of High-Grade Astrocytomas in Adults. Prog. Neurol. Surg 31, 116–144. [PubMed: 29393181]

Reardon DA, Nabors LB, Mason WP, Perry JR, Shapiro W, Kavan P, Mathieu D, Phuphanich S, Cseh A, Fu Y, et al. ; BI 1200 36 Trial Group and the Canadian Brain Tumour Consortium (2015). Phase I/randomized phase II study of afatinib, an irreversible ErbB family blocker, with or without protracted temozolomide in adults with recurrent glioblastoma. Neuro-oncol. 17, 430–439. [PubMed: 25140039]

Regala RP, Weems C, Jamieson L, Copland JA, Thompson EA, and Fields AP (2005a). Atypical protein kinase Ciota plays a critical role in human lung cancer cell growth and tumorigenicity. J. Biol. Chem 280, 31109–31115. [PubMed: 15994303]

Regala RP, Weems C, Jamieson L, Khoor A, Edell ES, Lohse CM, and Fields AP (2005b). Atypical protein kinase C iota is an oncogene in human non-small cell lung cancer. Cancer Res. 65, 8905–8911. [PubMed: 16204062]

Regala RP, Thompson EA, and Fields AP (2008). Atypical protein kinase C iota expression and aurothiomalate sensitivity in human lung cancer cells. Cancer Res. 68, 5888–5895. [PubMed: 18632643]

Regala RP, Davis RK, Kunz A, Khoor A, Leitges M, and Fields AP (2009). Atypical protein kinase Ciota is required for bronchioalveolar stem cell expansion and lung tumorigenesis. Cancer Res. 69, 7603–7611. [PubMed: 19738040]

Reilly KM, Loisel DA, Bronson RT, McLaughlin ME, and Jacks T (2000). Nf1;Trp53 mutant mice develop glioblastoma with evidence of strain-specific effects. Nat. Genet 26, 109–113. [PubMed: 10973261]

Roder C, and Thomson MJ (2015). Auranofin: repurposing an old drug for a golden new age. Drugs R D. 15, 13–20. [PubMed: 25698589]

Scotti ML, Bamlet WR, Smyrk TC, Fields AP, and Murray NR (2010). Protein kinase Ciota is required for pancreatic cancer cell transformed growth and tumorigenesis. Cancer Res. 70, 2064–2074. [PubMed: 20179210]

Scotti ML, Smith KE, Butler AM, Calcagno SR, Crawford HC, Leitges M, Fields AP, and Murray NR (2012). Protein kinase C iota regulates pancreatic acinar-to-ductal metaplasia. PLoS ONE 7, e30509. [PubMed: 22359542]

Sonabend AM, Yun J, Lei L, Leung R, Soderquist C, Crisman C, Gill BJ, Carminucci A, Sisti J, Castelli M, et al. (2013). Murine cell line model of proneural glioma for evaluation of anti-tumor therapies. J. Neurooncol 112, 375–382. [PubMed: 23504257]

Stallings-Mann M, Jamieson L, Regala RP, Weems C, Murray NR, and Fields AP (2006). A novel small-molecule inhibitor of protein kinase Ciota blocks transformed growth of non-small-cell lung cancer cells. Cancer Res. 66, 1767–1774. [PubMed: 16452237]

Subramanian A, Tamayo P, Mootha VK, Mukherjee S, Ebert BL, Gillette MA, Paulovich A, Pomeroy SL, Golub TR, Lander ES, and Mesirov JP (2005). Gene set enrichment analysis: a knowledge-based approach for interpreting genome-wide expression profiles. Proc. Natl. Acad. Sci. USA 102, 15545–15550. [PubMed: 16199517]

Szerlip NJ, Pedraza A, Chakravarty D, Azim M, McGuire J, Fang Y, Ozawa T, Holland EC, Huse JT, Jhanwar S, et al. (2012). Intratumoral heterogeneity of receptor tyrosine kinases EGFR and PDGFRA amplification in glioblastoma defines subpopulations with distinct growth factor response. Proc. Natl. Acad. Sci. USA 109, 3041–3046. [PubMed: 22323597]

Verhaak RG, Hoadley KA, Purdom E, Wang V, Qi Y, Wilkerson MD, Miller CR, Ding L, Golub T, Mesirov JP, et al. ; Cancer Genome Atlas Research Network (2010). Integrated genomic analysis identifies clinically relevant subtypes of glioblastoma characterized by abnormalities in PDGFRA, IDH1, EGFR, and NF1. Cancer Cell 17, 98–110. [PubMed: 20129251]

Wang Y, Hill KS, and Fields AP (2013). PKCι maintains a tumor-initiating cell phenotype that is required for ovarian tumorigenesis. Mol. Cancer Res 11, 1624–1635. [PubMed: 24174471]

Wang Z, Sun D, Chen YJ, Xie X, Shi Y, Tabar V, Brennan CW, Bale TA, Jayewickreme CD, Laks DR, et al. (2020). Cell Lineage-Based Stratification for Glioblastoma. Cancer Cell 38, 366–379.e8. [PubMed: 32649888]

Wang LB, Karpova A, Gritsenko MA, Kyle JE, Cao S, Li Y, Rykunov D, Colaprico A, Rothstein JH, Hong R, et al. ; Clinical Proteomic Tumor Analysis Consortium (2021). Proteogenomic and metabolomic characterization of human glioblastoma. Cancer Cell 39, 509–528.e20. [PubMed: 33577785]

Yin N, Liu Y, Khoor A, Wang X, Thompson EA, Leitges M, Justilien V, Weems C, Murray NR, and Fields AP (2019). Protein Kinase Cι and Wnt/β-Catenin Signaling: Alternative Pathways to Kras/Trp53-Driven Lung Adenocarcinoma. Cancer Cell 36, 156–167.e7. [PubMed: 31378680]

Yin N, Liu Y, Murray NR, and Fields AP (2020). Oncogenic protein kinase Cι signaling mechanisms in lung cancer: Implications for improved therapeutic strategies. Adv. Biol. Regul 75, 100656. [PubMed: 31623973]

Yuan J, Levitin HM, Frattini V, Bush EC, Boyett DM, Samanamud J, Ceccarelli M, Dovas A, Zanazzi G, Canoll P, et al. (2018). Single-cell transcriptome analysis of lineage diversity in high-grade glioma. Genome Med. 10, 57. [PubMed: 30041684]

Highlights

- PKCι is an oncogenic driver of GBM that confers response to PKCι inhibitor therapy
- GBMs can be classified into mutually exclusive PKCι- or SRC-dependent subtypes
- PKCι- and SRC-dependent cells often co-exist in single GBM tumors
- Combined PKCι and SRC inhibition is an effective treatment strategy for GBM

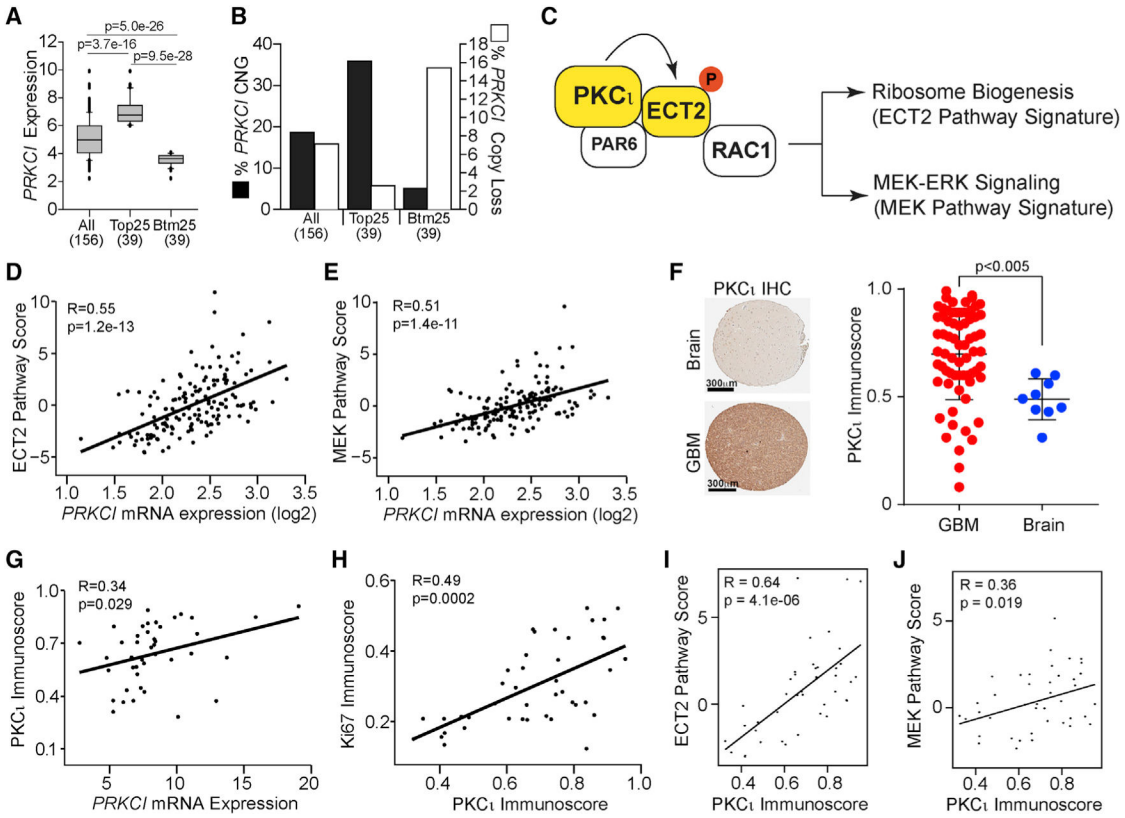

Figure 1. Characterization of PKCι signaling in human GBM tumors

(A) Expression of *PRKCI* mRNA in human GBM from TCGA dataset. Results are plotted for all tumor samples (All, n = 156), for the 25% expressing the highest *PRKCI* (Top25, n = 39), and for the 25% lowest *PRKCI* (Btm25, n = 39). Boxes indicate the median, 25%, and 75% confidence intervals, and error bars indicate 95% confidence interval. Significance was assessed by unpaired two-tailed t test.

(B) Prevalence and distribution of *PRKCI* copy number alterations in GBM tumors. Data represent the percentage of all tumor samples (n = 156), *Top25* (n = 39), and *Btm25* (n = 39) harboring either *PRKCI* copy number gain (black bars, GISTIC score +1, left y axis) or monoallelic *PRKCI* loss (white bars, GISTIC score −1, right y axis). Significant differences in *PRKCI* copy number alterations were assessed by chi-square analysis.

(C) Schematic showing two well-characterized oncogenic pathways activated by PKCι-ECT2-RAC1 signaling. Gene signatures associated with each pathway were used to interrogate pathway activity.

(D and E) Plot of ECT2 (D) and MEK (E) pathway scores versus *PRKCI* mRNA expression in all TCGA GBMs.

(F) Representative PKCι IHC from normal brain (frontal cortex and subjacent white matter) and GBM tissues from a human TMA (left panel). PKCι immunoscores for 68 GBM (red) and 9 normal brain (blue) samples from the TMA are plotted (right panel). Bars represent mean ± 1 SD. Statistical significance was determined by two-tailed t test.

(G and H) Plots of PKCι immunoscore versus *PRKCI* mRNA expression (G) and Ki67 immunoscore (H) in human GBM PDX models (n = 42).

(I and J) Plot of *ECT2* (I) and *MEK* (J) pathway scores versus PKCι immunoscore in human GBM PDX models (n = *42*). Spearman correlation coefficient (R) and significance (p value) are indicated in (D), (E), and (G)–(J).

See also Figures S1–S3 and Table S1.

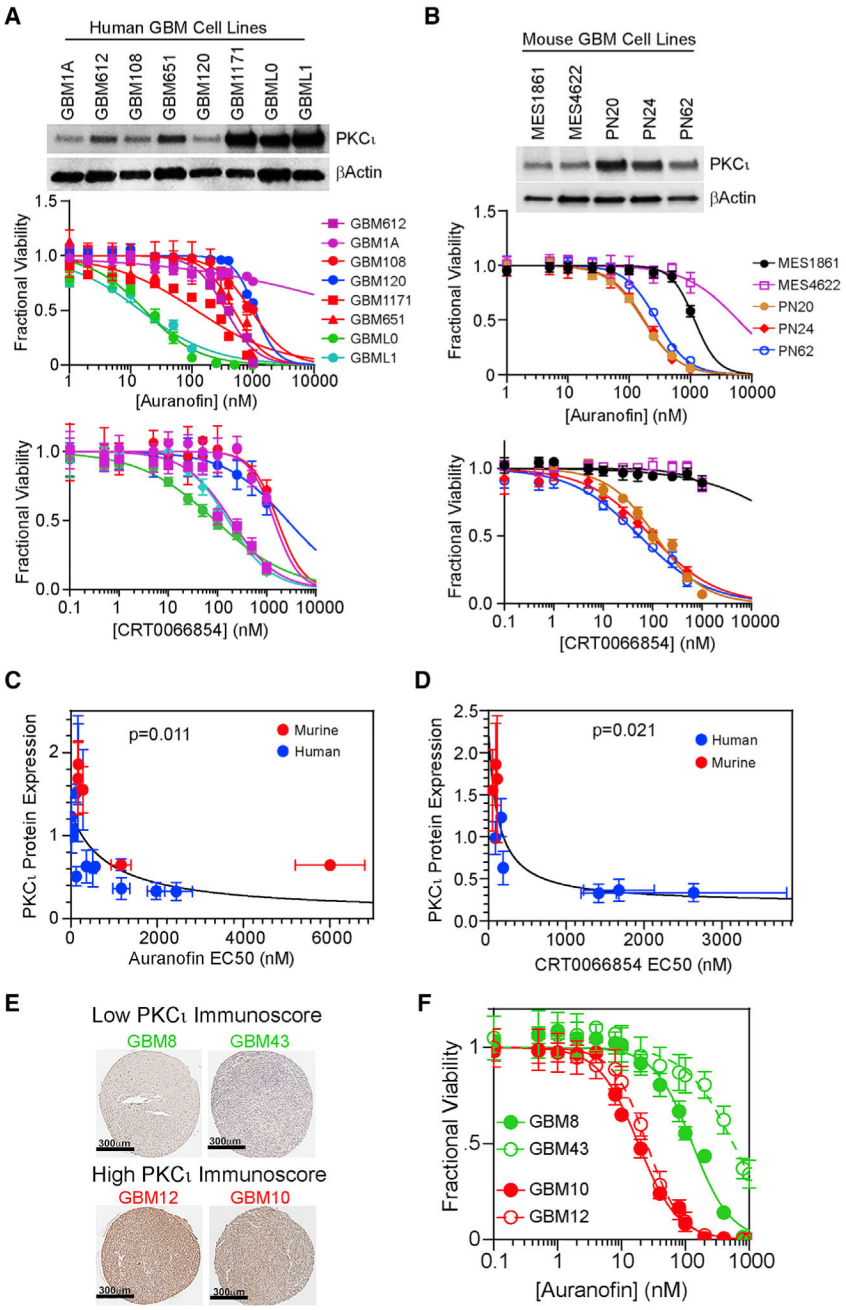

Figure 2. Effect of PKCι inhibitors on mouse and human GBM cell lines

(A and B) Human (A) and murine (B) GBM cell lines were assessed for expression of PKCι by immunoblot analysis using β-Actin as a loading control (upper panels) and for the effect of auranofin (middle panels) and CRT006854 (lower panels) on cell viability. Each point represents the mean ± 1 SD from 8 replicates.

(C and D) Plot of auranofin (C) and CRT0066854 (D) EC_{50}s versus PKCι expression in murine (red) and human (blue) GBM cell lines, fit to hyperbolic functions (solid red and blue lines). The significance (p value) is indicated in (C) and (D). Each point represents the mean ± 1 SD from 2–4 replicates.

(E) IHC detection of PKCι in representative human PDX-derived GBM cell lines demonstrating low (*GBM8* and *GBM43*, top) or high (*GBM12* and *GBM10*, bottom) PKCι immunoscores.

(F) Auranofin dose-response curves for low PKCι (*GBM8* and *GBM43*, green curves) and high PKCι (*GBM12* and *GBM10*, red curves) cell lines. Each point represents the mean ± 1 SD from 8 replicates.

See also Table S2 and Figure S2.

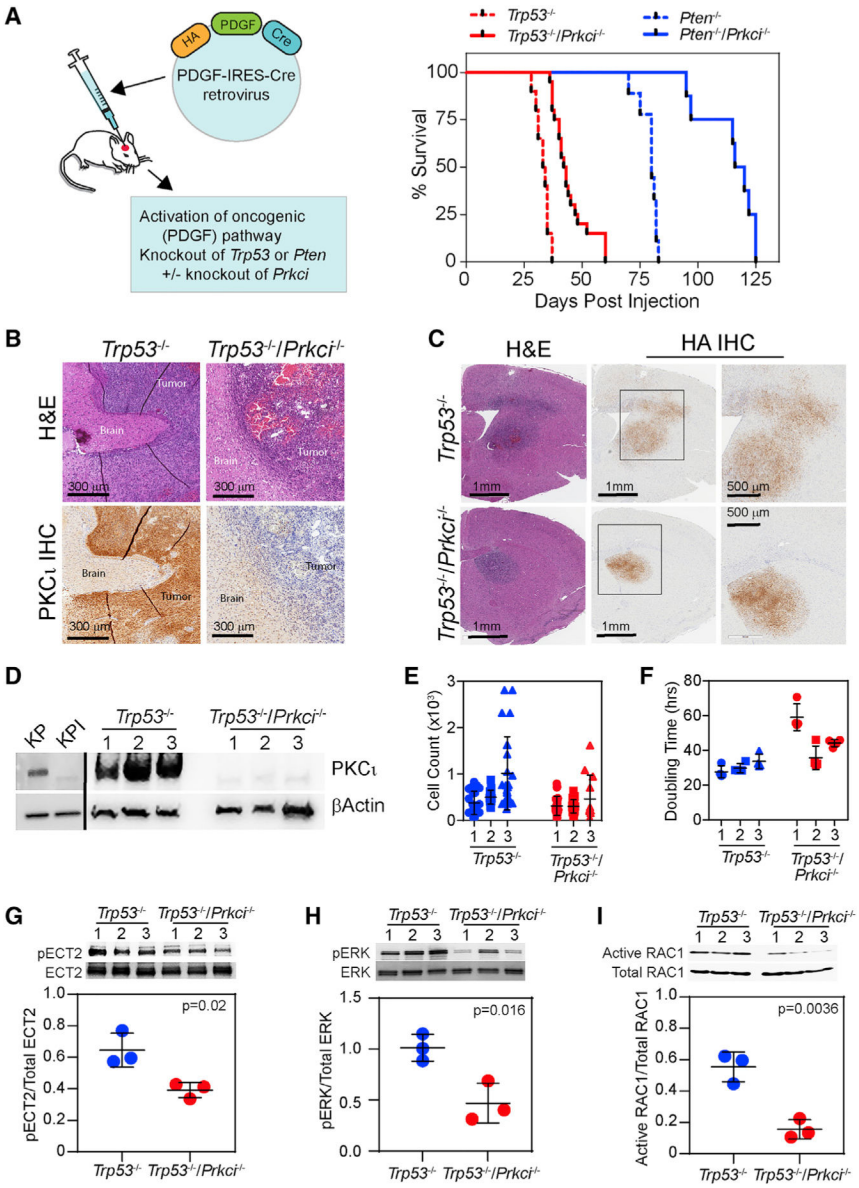

Figure 3. Effect of *Prkci* deletion on GBM tumorigenesis

(A) Schematic of the GEMMs used in this study (left panel). Kaplan-Meier survival curves of *Trp53*$^{fl/fl}$, *Trp53*$^{fl/fl}$/*Prkci*$^{fl/fl}$, *Pten*$^{fl/fl}$, and *Pten*$^{fl/fl}$/*Prkci*$^{fl/fl}$ tumor-bearing mice (right panel) (median survival: 31 versus 43 days for *Trp53*$^{-/-}$ versus *Trp53*$^{-/-}$/*Prkci*$^{-/-}$ mice, $p < 0.0001$; median survival: 80 versus 115 days for *Pten*$^{-/-}$ versus *Pten*$^{-/-}$/*Prkci*$^{-/-}$ mice, $p < 0.0001$; 10 mice/group). Significance was assessed by log rank test.

(B and C) *Trp53*-deleted and *Trp53*/*Prkci* co-deleted tumors were harvested at endpoint (B) or at 14 days after tumor initiation (C), and sections stained with H&E or HA and PKCι were detected by IHC as indicated. Areas in (C) circumscribed by black boxes are shown at higher magnification in the right panels.

(D) Immunoblot for PKCι in three *Trp53*$^{-/-}$ and three *Trp53*$^{-/-}$/*Prkci*$^{-/-}$ cell lines established from murine GBMs. KP and KPI cells are included as positive and negative controls for PKCι expression (Yin et al., 2019), respectively.

(E) Three independent *Trp53*$^{-/-}$ (blue) and *Trp53*$^{-/-}$/*Prkci*$^{-/-}$ (red) cell lines were evaluated for invasive capacity through 3-μm Transwells. Bars represent mean ± 1 SD from 8 replicates.

(F) Three replicates of three independent *Trp53*$^{-/-}$ (blue) and *Trp53*$^{-/-}$/*Prkci*$^{-/-}$ (red) GBM cell lines were grown on fibronectin-coated plastic dishes, and cell count was monitored to calculate doubling times. Bars represent mean ± 1 SD.

(G and H) Three biological replicates of lysates from *Trp53*$^{-/-}$ and *Trp53*$^{-/-}$/*Prkci*$^{-/-}$ cell lines were subjected to immunoblot analysis for phospho-T328 and total ECT2 (G) and phospho-ERK and total ERK (H) (upper panels). The ratio of phosphorylated to total protein is plotted (lower panels).

(I) Active and total RAC1 were measured in *Trp53*$^{-/-}$ and *Trp53*$^{-/-}$/*Prkci*$^{-/-}$ GBM lysates (top panels). The ratio of active to total RAC1 is plotted (bottom panels). Significance in (G)–(I) was determined by two-tailed t test. Bars represent mean ± 1 SD for 3 replicates.

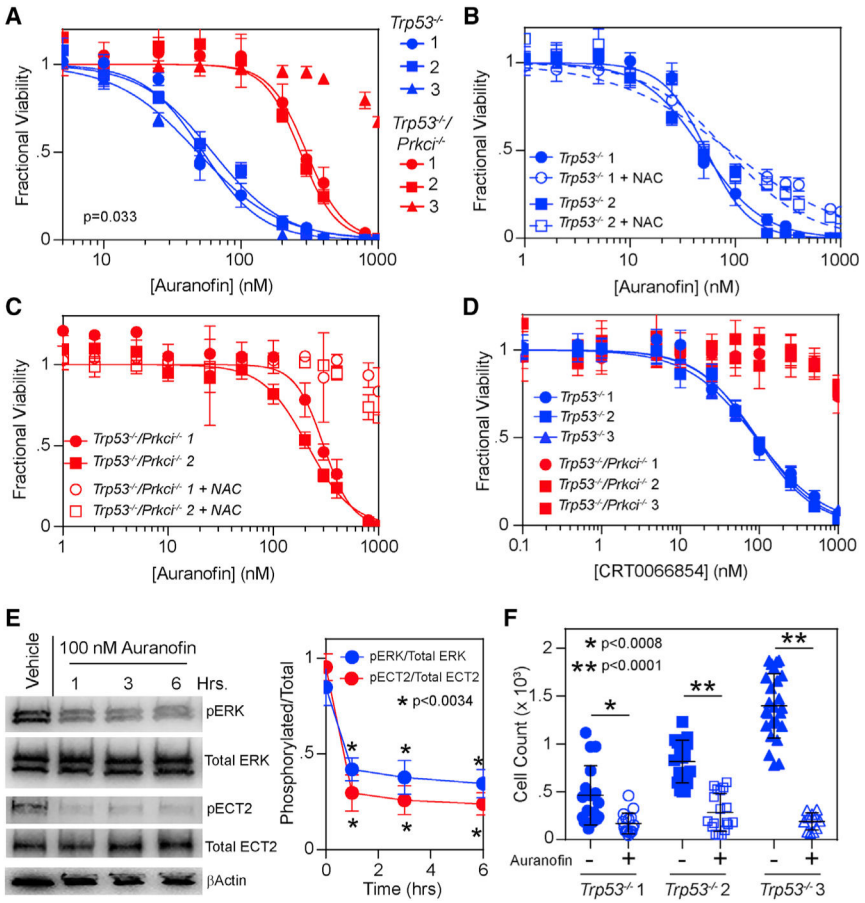

Figure 4. Effect of PKCι inhibitors on GBM cell viability and PKCι signaling

(A) *Trp53*$^{-/-}$ and *Trp53*$^{-/-}$/*Prkci*$^{-/-}$ GBM cells grown were treated with auranofin for 72 h. Each point represents the mean ± 1 SD from 10 replicates.

(B and C) *Trp53*$^{-/-}$ (B) and *Trp53*$^{-/-}$/*Prkci*$^{-/-}$ (C) cells were treated with auranofin ± 2 mM *N*-acetyl cysteine (*NAC*), and cell viability was assessed. Each point represents the mean ± 1 SD from 10 replicates. Data in (A)–(C) were fit to the Hill equation, constrained to eliminate data from the top and bottom 5% of drug concentrations to improve curve fitting.

(D) *Trp53*$^{-/-}$ and *Trp53*$^{-/-}$/*Prkci*$^{-/-}$ cells grown in 96-well plates were treated with CRT0066854 for 72 h. For (A)–(D), each point represents the mean ± 1 SD from 8 replicates.

(E) *Trp53*$^{-/-}$ cells (line 1) were treated with vehicle for 6 h or with 100 nM auranofin for 1, 3, and 6 h, and levels of total and phospho-ECT2 and ERK were measured by immunoblot (left panel). Band intensity is plotted as phospho-ERK/total ERK and phospho-ECT2/total ECT2 (right panel). Each point represents the mean ± 1 SD from 3 replicates. Significance was assessed by pairwise t test compared with the t = 0 vehicle control.

(F) Invasion of *Trp53*$^{-/-}$ cells through 3-μm Transwell membranes was measured in the presence of vehicle (closed) or 100 nM auranofin (open). Bar represents the mean ± 1 SD from 8 replicates. Significance was determined by two-tailed t test.

See also Table S2 and Figure S4.

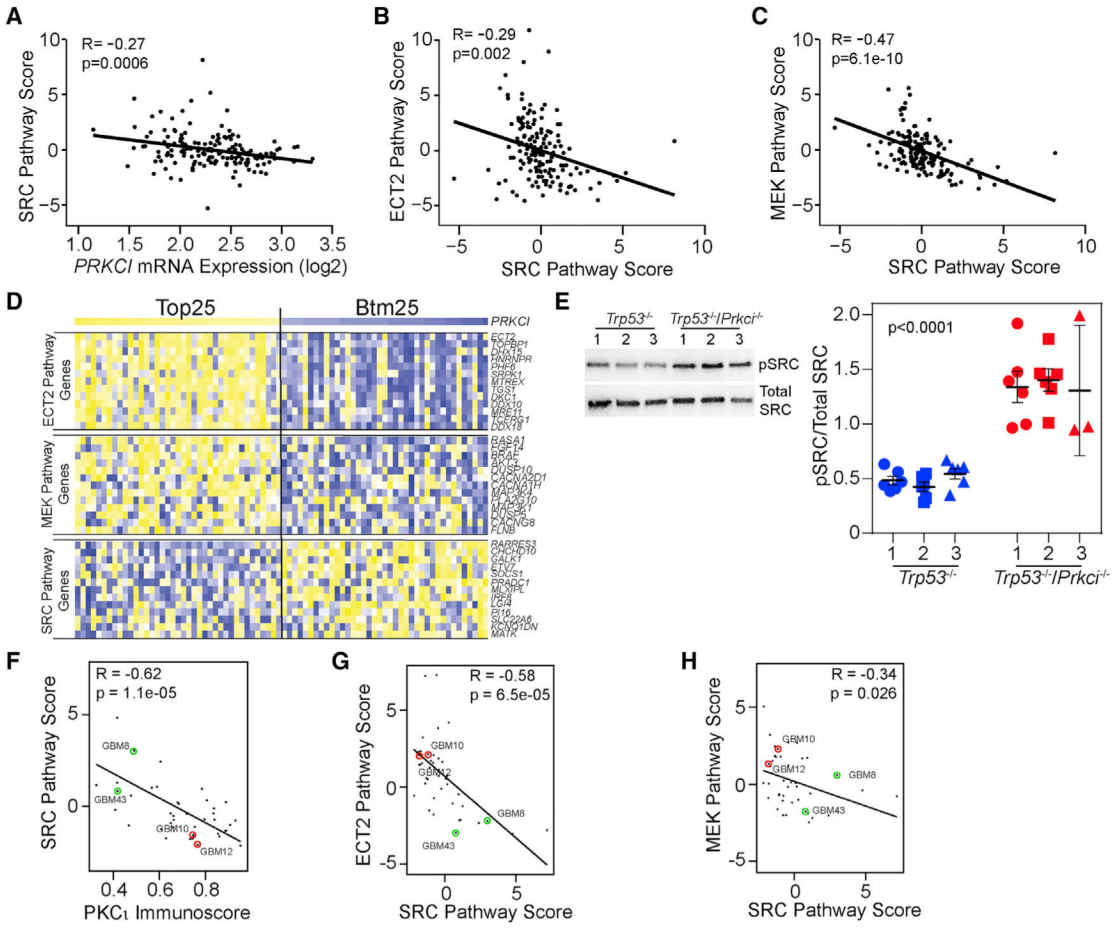

Figure 5. SRC signaling is activated in GBMs expressing low *PRKCI*

(A–C) Scatterplots showing the relationship between *SRC* pathway score and *PRKCI* expression (A), *ECT2* pathway score (B), and *MEK* pathway score (C) in TCGA GBM samples (n = 156).

(D) Heatmap depicting relative mRNA expression (from TCGA) of the classifier genes constituting the *ECT2* (top panels), *MEK* (middle panels), and *SRC* (bottom panels) pathway signatures in the *Top25* (left panels) and *Btm25* (right panels) groups.

(E) Immunoblot for phosphorylated (pY418) and total SRC in three independent $Trp53^{-/-}$ and $Trp53^{-/-}/Prkci^{-/-}$ GBM cell lines (left panel). Quantification of immunoblot results plotted for each cell line as the mean ± 1 SD (right panel). Differences between the genotypes are significant (n = 3–6 per cell line; $p < 0.0001$, one-way ANOVA).

(F–H) Scatterplots depicting the relationship between *SRC* pathway score and PKCι immunoscore (F), *ECT2* pathway score (G), and *MEK* pathway score (H) in human PDX-derived GBM cell lines. The two high and two low PKCι-expressing cells shown in Figure 2 are indicated in red and green, respectively.

(A–C and F–H) Spearman correlation coefficient (R) and significance (p value) are given. See also Table S3 and Figure S4.

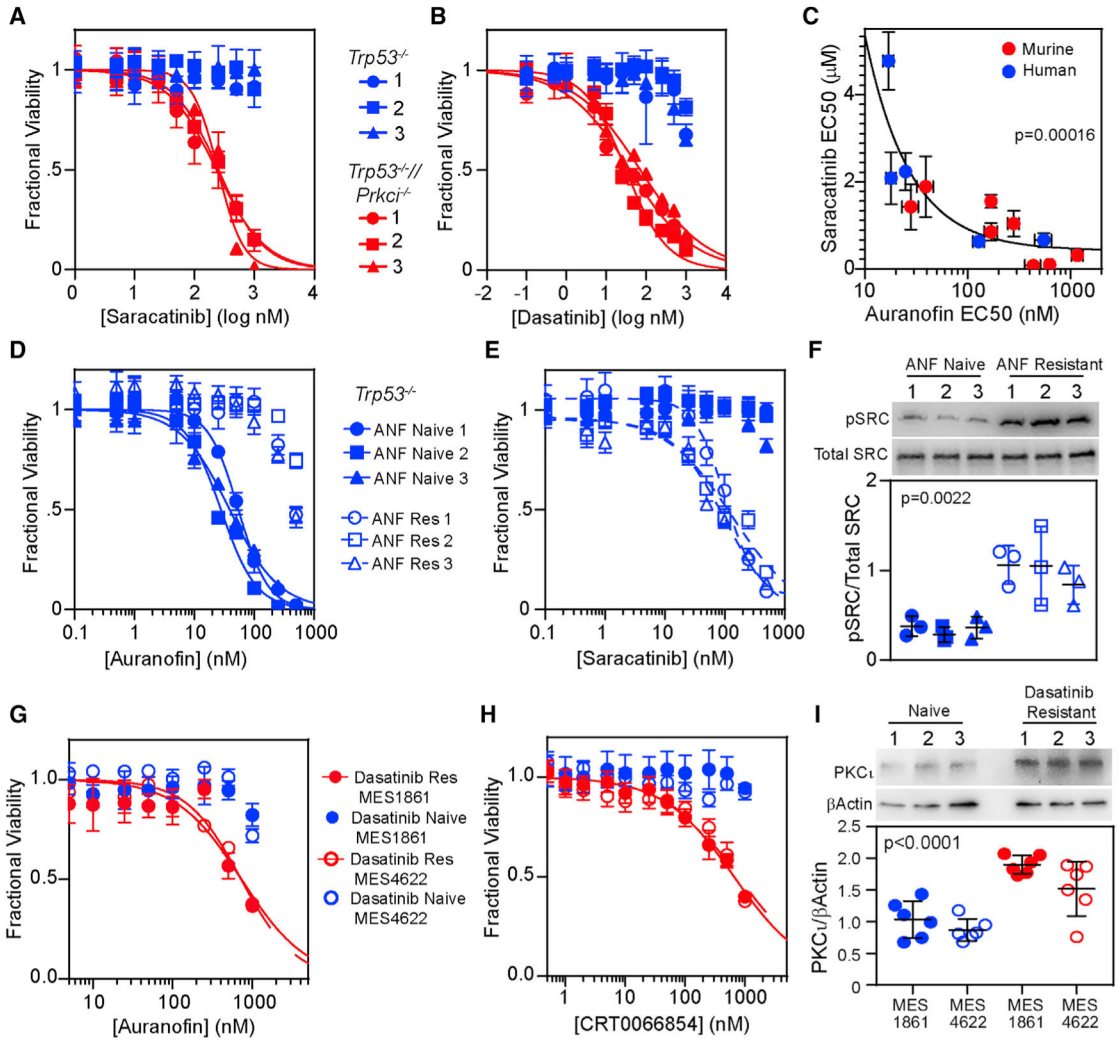

Figure 6. Reciprocal relationship between PKCι and SRC inhibitor sensitivities in GBM cells

(A and B) *Trp53*$^{-/-}$ (blue) and *Trp53*$^{-/-}$/*Prkci*$^{-/-}$ (red) murine GBM cells were treated with saracatinib (A) and dasatinib (B) for 72 h. Each point represents the mean ± 1 SD from 8 replicates.

(C) A plot of saracatinib EC_{50} versus auranofin (ANF) EC_{50} for eight human (red) and five murine (blue) GBM cell lines fit to rectangular hyperbolae (red and blue solid curves). Error bars indicate mean ± SEM. Statistical significance (p value) is indicated.

(D and E) Dose-response curves of ANF (D) and saracatinib (E) in ANF-naive (closed symbols) and ANF-resistant (open symbols) *Trp53*$^{-/-}$ GBM cells. Each point represents the mean ± 1 SD from 8 replicates.

(F) (Top panel) Immunoblot of ANF-naive and -resistant cells for phosphorylated pY418 SRC and total SRC. (Bottom panel) Quantification of phospho-SRC for both ANF-naive and -resistant GBM cell lines. Results are expressed as pSRC/total SRC, and each point represents the mean ± 1 SD from 3 replicates.

(G and H) Dose-response curves to ANF (G) and CRT0066854 (H) treatment of drug-naive and dasatinib-resistant MES1861 and MES4622 GBM cells. Each point represents the mean ± 1 SD from 8 replicates.

(I) (Top panel) Representative immunoblots of lysates derived from three cultures of dasatinib-naive and -resistant MES1861cells for PKCι and actin. (Bottom panel) Quantification of PKCι expression by immunoblot analysis in dasatinib-naive and -resistant MES1861 and MES4622 GBM cells. Results are expressed as PKCι/β-Actin, and each point represents the mean ± 1 SD from 6 replicates.
See also Table S2 and Figure S5.

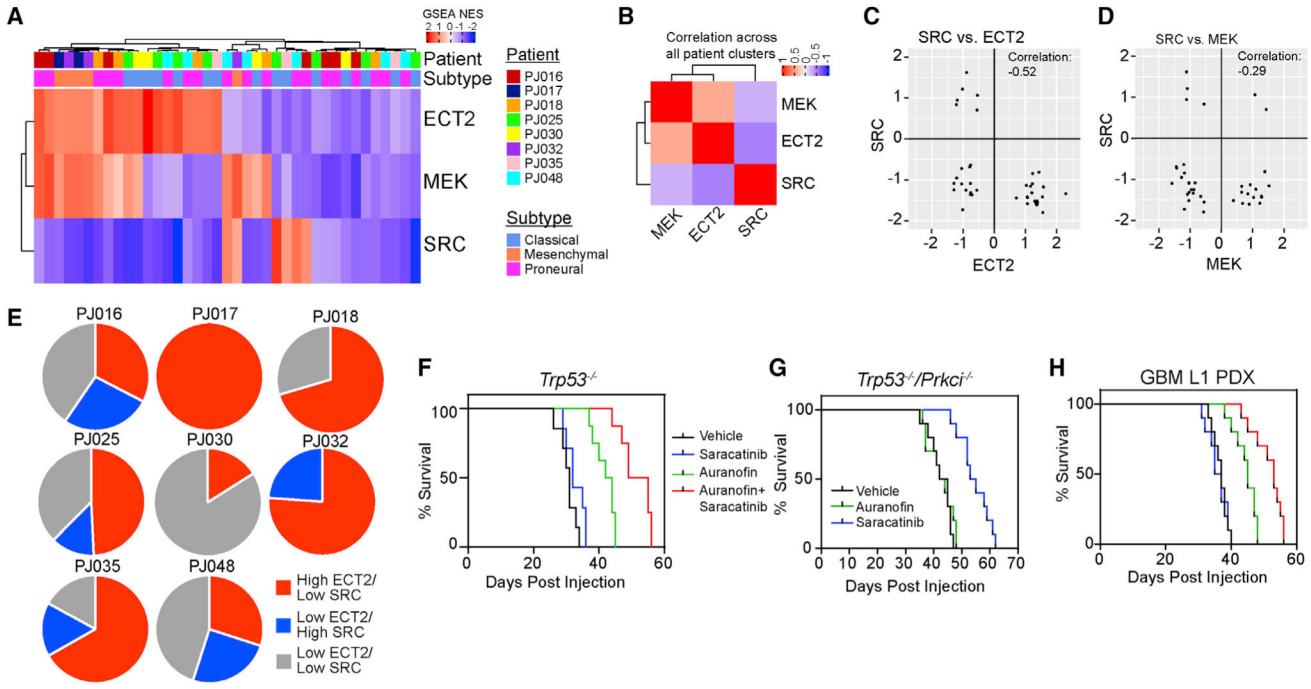

Figure 7. Human GBMs harbor distinct PKCι- or SRC-dependent tumor cell populations

(A) Heatmap of *ECT2*, *MEK*, and *SRC* pathway scores arranged via hierarchical clustering, with each tumor cell cluster annotated by patient ID and Verhaak tumor subtype.

(B) Heatmap of Spearman correlation matrix comparing *MEK*, *ECT2*, and *SRC* pathway scores across tumor cell clusters from eight high-grade glioma patient tumors. Each cell represents a Spearman rank correlation coefficient, and the heatmap is arranged via hierarchical clustering.

(C and D) Scatterplot comparing *SRC* and *ECT2* pathway scores (C) or *SRC* and *MEK* pathway scores (D) from all tumor cell clusters in the eight-patient cohort. The Spearman correlation coefficient is indicated.

(E) Pie charts indicating the relative abundance of high ECT2/low SRC (red), low ECT2/ high SRC (blue), and low ECT2/low SRC (gray) tumor cells in each tumor from the GBM cohort.

(F) Kaplan-Meier curves showing survival of $Trp53^{-/-}$ mice with GBM tumors treated with vehicle, saracatinib, auranofin, or auranofin + saracatinib starting 5 days after retroviral injection. Significant differences in median survival were observed between vehicle and auranofin ($p < 0.0001$) and between auranofin and auranofin + saracatinib ($p = 0.0004$), but not between vehicle and saracatinib ($p = 0.095$). Seven to eight mice per group.

(G) GBM tumorigenesis was initiated in $Trp53^{fl/fl}/Prkci^{fl/fl}$ mice, which were treated with vehicle, saracatinib, or auranofin as in (F). Kaplan-Meier analysis demonstrates significant differences in median survival between vehicle and saracatinib ($p < 0.0001$), but not between vehicle and auranofin ($p = 0.52$). Ten mice per group.

(H) Non-obese diabetic severe combined immunodeficiency (NOD-SCID) mice were orthotopically injected with 100,000 human GBM L1 cells, and 20 days later were treated with vehicle, saracatinib, auranofin, or auranofin + saracatinib as in (F). Kaplan-Meier analysis demonstrates significant differences in median survival between vehicle and

auranofin ($p < 0.0001$) and between auranofin and auranofin + saracatinib ($p = 0.0012$), but not between vehicle and saracatinib ($p = 0.85$). n = 10 mice/treatment group. Significance was assessed in (F)–(H) by log rank test.

KEY RESOURCES TABLE

REAGENT or RESOURCE	SOURCE	IDENTIFIER
Antibodies		
Rat monoclonal Anti-HA (clone 3F10)	Sigma-Aldrich	Cat#11867423001; RRID: AB_390918
Rabbit polyclonal anti-Ki67	Vector Laboratories	Cat# VP-K451; RRID: AB_2314701
Mouse monoclonal anti-PKCi	BD Biosciences	Cat# 610176, RRID: AB_397575
Rabbit polyclonal anti-ECT2	Millipore	Cat# 07-1364, RRID: AB_10805932
Mouse monoclonal anti-Rac1 (clone102)	BD Biosciences	Cat# 610651, RRID: AB_397978
Rabbit polyclonal anti-Phospho-Src (Tyr418)	Millipore	Cat# 07-909; RRID: AB_568805
Rabbit polyclonal anti-Src	Cell Signaling Technology	Cat# 2108; RRID: AB_331137
Rabbit anti-p44/42 MAPK (Erk1/2)	Cell Signaling Technology	Cat# 9102; RRID: AB_330744
Rabbit monoclonal anti-Phospho-p44/42 MAPK (Erk1/2) (Thr202/Tyr204)	Cell Signaling Technology	Cat# 4370; RRID: AB_2315112
Rabbit monoclonal anti-Phospho-EGF Receptor (Tyr1068) (D7A5)	Cell Signaling Technology	Cat# 3777; RRID: AB_2096270
Rabbit polyclonal anti-EGF Receptor	Cell Signaling Technology	Cat# 2232; RRID: AB_331707
Mouse monoclonal anti-β-Actin (8H10D10)	Cell Signaling Technology	Cat# 3700; RRID: AB_2242334
Rabbit polyclonal anti-Phospho-cABL (Tyr245)	Thermo Fisher Scientific	Cat# PA5-12532; RRID: AB_10978518
Rabbit polyclonal anti-cABL	Cell Signaling Technology	Cat# 2862; RRID: AB_2257757
Rabbit polyclonal anti-Phospho-Lyn (Tyr507)	Cell Signaling Technology	Cat# 2731; RRID: AB_2138262
Rabbit anti-Lyn	Cell Signaling Technology	Cat# 2732; RRID: AB_10694080
Rabbit polyclonal anti-Phospho-FYN (Y530)	Abcam	Cat#Ab182661
Rabbit polyclonal anti-FYN	Cell Signaling Technology	Cat# 4023; RRID: AB_10698604
Rabbit anti-Phospho-Thr-328-ECT2	21st Century Biochemicals	(Justilien et al., 2011)
Bacterial and virus strains		
PDGF-IRES-Cre retrovirus	Lei et al., 2011; Kenchappa et al., 2020	N/A
Biological samples		
Human GBM TMAs	Mayo Clinic Brain Tumor Patient Derived Xenograft National Resources	https://www.mayo.edu/research/labs/translational-neuro-oncology/mayo-clinic-brain-tumor-patient-derived-xenograft-national-resource/overview
Chemicals, peptides, and recombinant proteins		
PDGF-AA	Peprotech	Cat# 100-13A
hFGF (Human Fibroblast Growth factor)	R&D systems	Cat# 233-FB-025
hEGF (Human Epidermal Growth Factor)	Sigma-Aldrich	Cat# E9644
Fibronectin	Millipore-Sigma	Cat# FC010
Heparin	STEMCELL Technologies	Cat# 07980
N2 supplement	GIBCO life technologies	Cat# 17502-048
NeuroPlex supplement	Gemini	Cat# 400-161
Auranofin	Santa Cruz Biotechnology	Cat# SC202476A

REAGENT or RESOURCE	SOURCE	IDENTIFIER
Saracatinib	Selleck Chemicals	Cat# S1006
Dasatinib	Selleck Chemicals	Cat# S1021
Erlotinib	Selleck Chemicals	Cat# S7786
CRT0066854	Tocris Bioscience	Cat# 5922
N-Acetyl-L- cysteine	Santa Cruz Biotechnology	Cat# SC-202232A
Fluoroblok transwell inserts	Corning	Cat# 351151
VECTASHIELD with DAPI	Vector Laboratories	Cat# U-1500
Formaldehyde, 10% methanol free	CHEM (VWR)	Cat# 87001-890
SUPER signal West Pico PLUS Chemiluminescent substrate	Thermo Fisher Scientific	Cat# 34580
PBS	Thermo Fisher Scientific	Cat# 21-040
PVDF membrane	Biorad	Cat# 1620174
DMSO	Corning	Cat# 25-950-cqc
BSA	Thermo Fisher Scientific	Cat# 23209
Non-fat dry milk (Blotting grade blocker)	Biorad	Cat# 170-6404
Accutase	Sigma-Aldrich	Cat# A6964-500
Ethanol	Thermo Fisher Scientific	Cat# 61500-0020
Tween 20	Sigma-Aldrich	Cat# P1379
TBS	Thermo Fisher Scientific	Cat# 28358
Protease Inhibitor Cocktail, EDTA-free (100X)	Thermo Fisher Scientific	Cat# 87785
Pierce T-1step transfer buffer	Thermo Fisher Scientific	Cat# 84731
Western blot striping buffer	Thermo Fisher Scientific	Cat# 46430
10X Tris/Glycine/SDS buffer	Biorad	Cat# 1610772
Geltrex	GIBCO	Cat# A14132-01
Laminin	Thermo Fisher Scientific	Cat# 3400-010-02
RIPA lysis buffer	Thermo Fisher Scientific	Cat# 89900
B27 supplement	Thermo Fisher Scientific	Cat# A3582801
Laemmli SDS Sample Buffer, reducing, 6X	Thermo Fisher Scientific	Cat# AAJ61337AC
Anti-Anti (100x)	GIBCO	Cat# 15240-062
Retrieval solution	Dako	Cat# S236784-2
Wash buffer	Dako	Cat# S300685-2C
Protein block	Dako	Cat# X090930-2
Antibody Diluent	Dako	Cat# S080983-2
Envision anti-mouse-HRP antibody	Dako	Cat# K400111-2
Envision anti-Rabbit-HRP antibody	Dako	Cat# K400311
Critical commercial assays		
CellTiter-Glo 2.0 assay kit	Promega	Cat# G9242
Pierce BCA Protein Assay Kit	Thermo Fisher Scientific	Cat# 23225
Deposited data		

REAGENT or RESOURCE	SOURCE	IDENTIFIER
RNA-seq data for tissue microarrays and patient derived xenografts.	Mayo Clinic Brain Tumor Patient Derived Xenograft National Resources	https://www.cbioportal.org/study/summary?id=gbm_mayo_pdx_sarkaria_2019
Single cell RNA-seq from human GBM samples	Columbia University	Accession #: GSE103224: https://www.ncbi.nlm.nih.gov/geo/query/acc.cgi?acc=GSE103224
Experimental models: Cell lines		
$Trp53^{-/-}$ #1	This paper	N/A
$Trp53^{-/-}$ #2	This paper	N/A
$Trp53^{-/-}$ #3	This paper	N/A
$Trp53^{-/-}$/$Prkci^{-/-}$ #1	This paper	N/A
$Trp53^{-/-}$/$Prkci^{-/-}$ #2	This paper	N/A
$Trp53^{-/-}$/$Prkci^{-/-}$ #3	This paper	N/A
GBM1A	Galli et al., 2004	N/A
GBML1	Deleyrolle et al., 2011	N/A
GBML0	Deleyrolle et al., 2011	N/A
GBM612	Kenchappa et al., 2020	N/A
GBM108	Gift from Dr. Quiñones-Hinojosa	N/A
GBM120	Kenchappa et al., 2020	N/A
GBM1171	Gift from Dr. Quiñones-Hinojosa	N/A
GBM651	Gift from Dr. Quiñones-Hinojosa	N/A
MES1861	Reilly et al., 2000; Gürsel et al., 2011	N/A
MES4622	Reilly et al., 2000; Gürsel et al., 2011	N/A
PN20	Hambardzumyan et al., 2009	N/A
PN24	Hambardzumyan et al., 2009	N/A
PN62	Hambardzumyan et al., 2009	N/A
GBM8	Mayo Clinic Brain Tumor Patient Derived Xenograft National Resources	N/A
GBM43	Mayo Clinic Brain Tumor Patient Derived Xenograft National Resources	N/A
GBM10	Mayo Clinic Brain Tumor Patient Derived Xenograft National Resources	N/A
GBM12	Mayo Clinic Brain Tumor Patient Derived Xenograft National Resources	N/A
Experimental models: Organisms/strains		
$Trp53^{fl/fl}$ mice	Jackson Laboratory	Stock# 008462
$Pten^{fl/fl}$ mice	Jackson Laboratory	Stock# 006440
$Prkci^{fl/fl}$ mice	Gift from Dr. Michael Leitges	Univ. Oslo
$Trp53^{fl/fl}$/$Prkci^{fl/fl}$ mice	This paper	N/A

REAGENT or RESOURCE	SOURCE	IDENTIFIER
$Pten^{fl/fl}/Prkci^{fl/fl}$ mice	This paper	N/A
NOD-SCID mice	Jackson Laboratory	Stock# 005557
Software and algorithms		
cBioportal for Cancer Genomics	Memorial Sloan Kettering Cancer Center	https://www.cbioportal.org/
Gene Set Enrichment Analysis (GSEA), hallmark analysis (version h.all.v7.0)	Broad Institute	https://www.gsea-msigdb.org/gsea/index.jsp
GraphPad Prism 7	GraphPad	https://www.graphpad.com/scientific-software/prism/
Aperio ScanScope ™ software	Leica Biosystems	https://www.leicabiosystems.com/digital-pathology/manage/aperio-imagescope/